Journal of Energy Chemistry 58 (2021) 170–197

Contents lists available at ScienceDirect

Journal of Energy Chemistry

journal homepage: www.elsevier.com/locate/jechem

http://www.journals.elsevier.com/journal-of-energy-chemistry/

Review

Polyimide separators for rechargeable batteries

Ziheng Lu [a,1,*], Fan Sui [a,1], Yue-E Miao [b,1], Guohua Liu [a], Cheng Li [a], Wei Dong [a], Jiang Cui [c], Tianxi Liu [b], Junxiong Wu [d,*], Chunlei Yang [a,*]

[a] Shenzhen Institutes of Advanced Technology, Chinese Academy of Sciences, Shenzhen 518055, Guangdong, China
[b] College of Materials Science and Engineering, Donghua University, Shanghai 201620, China
[c] Department of Materials Science and Engineering, Clemson University, Clemson, SC 29634, USA
[d] Department of Mechanical Engineering, The Hong Kong Polytechnic University, Hong Kong, China

ARTICLE INFO

Article history:
Received 3 July 2020
Revised 27 September 2020
Accepted 28 September 2020
Available online 7 October 2020

Keywords:
Polyimide
Lithium-ion batteries
Separators
Solid-state batteries
Molecular design

ABSTRACT

Separators are indispensable components of modern electrochemical energy storage devices such as lithium-ion batteries (LIBs). They perform the critical function of physically separating the electrodes to prevent short-circuits while permitting the ions to pass through. While conventional separators using polypropylene (PP) and polyethylene (PE) are prone to shrinkage and melting at relatively high temperatures (150 °C or above) causing short circuits and thermal runaway, separators made of thermally stable polyimides (PIs) are electrochemically stable and resistant to high temperatures, and possess good mechanical strength—making them a promising solution to the safety concerns of LIBs. In this review, the research progress on PI separators for use in LIBs is summarized with a special focus on molecular design and microstructural control. In view of the significant progress in advanced chemistries beyond LIBs, recent advances in PI-based membranes for applications in lithium-sulfur, lithium-metal, and solid-state batteries are also reviewed. Finally, practical issues are also discussed along with their prospects.

Contents

* Corresponding authors.
E-mail addresses: zh.lu1@siat.ac.cn (Z. Lu), jwuba@connect.ust.hk (J. Wu), cl.yang@siat.ac.cn (C. Yang).
[1] These authors contributed equally to this work.

https://doi.org/10.1016/j.jechem.2020.09.043

1. Introduction

Lithium-ion batteries (LIBs) have been proven as a transformative technology since their first commercial application in the 1990 s. Their properties, including high energy density, low self-discharge, good rate performance, and long shelf life, are desirable for energy storage [1–4]. With these superior characteristics, they have been dominating the market of portable electronics. However, despite their commercial success, research efforts are still underway to further improve this technology. With its ever-increasing growth over the past decade, the electric vehicle (EV) industry calls for high-power and high-energy–density LIBs with lower cost and improved safety.

A typical LIB consists of a cathode, an anode, and a liquid electrolyte between the two electrodes. In addition to these active components, an electron-insulating porous membrane is placed between the cathode and the anode to prevent direct contact between the two electrodes. Although such a separator is not electrochemically active, it significantly impacts the performance and durability of the battery [5]. An ideal separator is characterized by good electrochemical stability, high mechanical strength, good thermal resistivity, and high electrolyte uptake. These features are essential in ensuring that an LIB lasts long and delivers high power output during normal operation. More importantly, such separators prevent the battery from catching fire or exploding under harsh conditions. In current commercial LIBs, separators are mainly fabricated from polyolefins such as polyethylene (PE) and polypropylene (PP). Stretching is commonly employed during manufacturing to create microsized pores. These microporous polyolefin separators generally display good chemical stability and high porosity, and can be fabricated at a relatively low cost. However, they also suffer from inherent drawbacks: 1) the polyolefins are poorly wetted by ester carbonate electrolytes, and therefore the separators have to be modified either chemically or physically to ensure good affinity to liquid electrolytes; 2) the thermal stability of these separators is relatively poor. In fact, they are prone to shrinkage at ~ 130 °C and will melt at 150 °C or above. Thus, batteries using polyolefin separators are difficult to operate at temperatures higher than 130 °C, leading to significant safety concerns. For example, if the battery is subject to misuse or external impact, the polyolefin separators tend to degrade owing to the creation of a local hotspot. This often leads to internal short circuits and subsequent thermal runaway (TR). In extreme cases, explosions occur. Such safety issues caused by thermal instability are especially significant when the polyolefin separator is fabricated via the stretching process. Therefore, developing novel separators based on heat-resistant polymers is important.

Polyimide (PI) is a family of thermoset polymers that display excellent thermal stability. For example, Kapton®, the most successful commercial PI film product of Dupont since the 1970 s, is stable from −269 to 400 °C. Owing to their exceptional mechanical strength, good chemical stability, and high-temperature heat resistance, PIs have been applied in various fields that are of great technological importance, including but not limited to printed circuit boards, photovoltaic cells, and aerospace devices [6,7]. Over the past two decades, there has been an ever-increasing interest in the development of highly safe batteries owing to the boom in the use of EVs, where large battery packs are often incorporated. Developing PI-based separators that do not degrade at elevated temperatures is a promising direction for mitigating the safety issues of LIBs and has drawn considerable attention in both academia and the industry. Thus, various methods have been proposed to fabricate porous PI films suitable as separators in LIBs, including electrospinning, nonsolvent-induced phase inversion, and sacrificial templating [8–10]. Different designs, such as compositing with ceramics and polymers, have also been employed [11]. More importantly, PI-based membranes have also found applications in advanced batteries with chemistries beyond Li ions. Over the past decade, lithium-metal batteries (LMBs), lithium-sulfur batteries (LSBs), and solid-state batteries (SSBs) have been intensively studied owing to their extraordinary energy densities. PIs have been adopted as Li dendrite mitigators, Li polysulfide absorbers, and solid electrolytes in these systems. With these technological advancements, PI-based separators have become an important field that may not only greatly impact the safety of LIBs but also bring advanced battery chemistries up to commercial standards.

In this paper, we review the research progress of PI-based separators, as outlined in Fig. 1. We first introduce the molecular structures of PIs and discuss the design strategies used to achieve the desired physical/chemical properties. Then, we demonstrate the preparation and characteristics of various types of PI-based separators, including pure PI separators, PI-modified polymer sep-

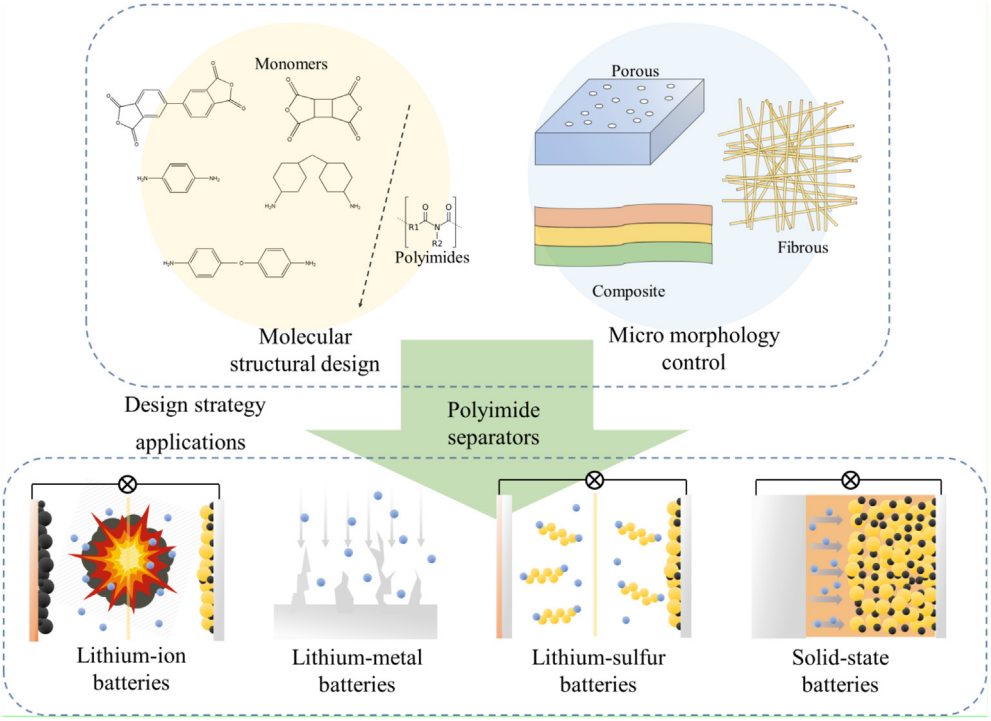

Fig. 1. Illustration of the outline of the review.

arators, and PI/ceramic composite separators. Their strengths and weaknesses are critically assessed in terms of their use in LIBs, with a special focus on safety performance. Common fabrication methods such as electrospinning, sacrificial templating, and phase inversion are discussed, with examples to facilitate an understanding of the preparation processes. Given the recent progress in advanced high-energy density chemistries beyond Li-ion, the use of PI-based separators in LMBs, LSBs, and SSBs are discussed as well, together with their molecular and microstructural design. Finally, a brief outlook is given on this promising field, with the most important practical aspects being addressed, such as large-scale production and cost issues. Because the current review covers not only most of the need-to-know knowledge, such as the fabrication methods of PI-based separators but also the more fundamental aspects, including the design strategies at the molecular level, it is beneficial to both junior researchers looking for references and chemists with extensive work experience in this field. In addition, we also expect that the fabrication methods and the design strategies of porous PI membranes as enclosed in this review will appeal to a broader community of polymer chemists, energy researchers, and engineers from the industry.

2. General requirements on separators for LIBs

Although separators are not active components in batteries, they play an important role in physically preventing contact between the cathode and the anode, and therefore they significantly influence the electrochemical performance, safety, and cost of the battery. Before providing a detailed discussion on PI-based separators, we briefly review the general requirements of separators for LIBs.

2.1. Chemical and electrochemical stability

Separators must be chemically and electrochemically stable toward electrolytes and electrode materials to avoid degradation and loss of mechanical strength. In addition, they should be stable against strong oxidizing and reducing conditions when the batteries are fully discharged and charged. Ideally, the electrochemical window of the dry membranes should be stable from 0 V to more than 5 V *vs.* Li/Li^+.

2.2. Electrolyte wettability

The wettability of the electrolyte to the membrane is another crucial property for battery separators because it affects the ion transport, which significantly affects the voltage hysteresis and rate capability of the battery. Separators must be able to absorb enough electrolyte to ensure low internal resistance and high ionic conductivity. The wettability of a separator depends on many factors, such as the chemical features of the surface of the polymer, the pore size, the porosity of the membrane, and the tortuosity of the microstructure [12,13]. Wettability of the electrolyte is strongly dependent on the type of electrolyte chosen. Currently, ester-type carbonates are the most commonly used electrolytes in commercial LIBs, and grafting hydrophilic groups onto the surface of the polymer usually leads to better wettability of the electrolyte. However, with the development of many other novel electrolyte systems, such as super-concentrated electrolytes and ionic liquid electrolytes, more investigation on electrolyte wettability is needed [14–17].

2.3. Porosity and pore sizes

The porosity of a separator determines the maximum electrolyte uptake. Therefore, a separator must be porous enough so that it can provide the desired Li^+ conductivity. Too low a porosity increases the internal resistance because of insufficient liquid electrolyte. However, if the porosity is too high, the mechanical stability will be significantly reduced, which causes potential safety concerns. Typically, commercial LIB separators have a porosity

of ~ 40%. The separator porosity can be calculated using the following equation [18]:

$$\text{Porosity}(\%) = \left(1 - \frac{\rho_M}{\rho_P}\right) \times 100\% \quad (1)$$

where ρ_M is the density of the separator and ρ_P is the density of the polymer. The porosity can also be estimated by weighing the separators before and after the absorption of the liquid electrolyte as follows [19]:

$$\text{Porosity}(\%) = \frac{W - W_0}{\rho_L V_0} \times 100\% \quad (2)$$

where W and W_0 are the weights of the separator before and after electrolyte absorption, respectively, and ρ_L and $V_0$are the density of the liquid electrolyte and the geometric volume of the separator, respectively.

In addition to the overall porosity, a homogenous pore-size distribution is also crucial. Nonuniform pores inevitably lead to inhomogeneous current density, thus reducing the battery performance. In practical cases, the sizes of the pores are within the sub-micrometer range, preventing internal short circuit in the battery due to penetration of the electrode materials and to some extent alleviating the unintentional Li metal deposition on the graphite anodes. Typically, mercury porosimetry is used to measure porosity, pore-size distribution, and mean pore size.

2.4. Permeability

The permeability of the separator describes how the geometric structure of the separator constricts Li^+ ion transport. For separators, the Gurley value, *G*, is generally used to describe permeability. The Gurley value is defined as the number of seconds required for a specific amount of air (100 cm^3) to pass through the unit area (1 $in.^2$) of the separator under a given pressure difference (1.21 kPa) [20]. The Gurley number is a good indicator of the properties of the separator. A low Gurley number means that the separator has high porosity and low tortuosity, which are advantageous for high-power batteries. To achieve good electrochemical performance and a long lifespan, the separator must have uniform permeability.

2.5. Mechanical properties

Tensile strength and puncture strength are used to characterize the mechanical properties of separators. A high tensile strength enables the separator to withstand tension during battery assembly, whereas a high puncture strength is needed to avoid short circuits caused by either the electrode materials or dendritic Li. For a 25-μm-thick separator, the minimum tensile strength should be 98 MPa based on the D882 and D638 standards of the American Society for Testing and Materials (ASTM), and the puncture strength should be higher than 300 g according to ASTM D3763 [13]. In general, a thin separator has a lower internal resistance but the lower mechanical strength. Therefore, the thickness and uniformity of the separators need fine control.

2.6. Thermal stability

The thermal stability of a separator is extremely important for batteries. Because most separators are made from polymers, especially polyolefins, which are prone to shrinkage and melt at relatively low temperatures (150 °C or above), short circuits and TR may occur. Generally, thermal shrinkage needs to be less than 5% after 60 min at 90 °C [21]. Recently, separators with shutdown behavior were developed to resolve electrical overcharging during battery operation [22,23]. Usually, these separators have a multilayer structure, where the middle layer has a relatively low melting point compared to the outer layers. When the temperature is higher than the TR temperature, the middle layer collapses and blocks the ion conduction. When these separators are used, the electrode reactions can be stopped in the batteries before an explosion occurs, thus enhancing the safety of batteries.

Table 1 compares some of the most critical physiochemical properties of the materials that are commonly used for separators in LIBs. PIs have much better thermal stability than polyolefins and polyvinylidene difluoride (PVDF). In addition, other separators with improved thermal stability have been reported for rechargeable batteries, including polysulfonamide [24], polyester [25,26], polyphthalazinone ether sulfone ketone (PPESK) [27], cellulose/polysulfonamide [28], and polyacrylonitrile [29,30]-based nonwoven membranes. These membranes not only showed high thermal stability but also exhibited high electrolyte uptake and high conductivity. However, the mechanical properties, thermal stability, and chemical stability of these nonwovens are still inferior to those of PI-based separators. Therefore, PIs are promising polymers for developing advanced separators. The detailed design principles of their molecular structures and the control of their micromorphologies are discussed in the following sections.

3. Molecular structures and properties of PI

3.1. General features of PI

PI is a polymer of imide monomers that are mostly known for their superior heat resistance. PIs are usually synthesized from two different types of monomers, i.e., diamines and dianhydrides. Some common chemical structures of diamine and dianhydride monomers taken from both industrial and research fields are shown in Fig. 2. For example, Dupont Kapton® films are produced from pyromellitic dianhydride (PMDA) and 4,4′-oxydianiline (ODA) monomers, and Ube Upilex® films are made of 3,3,4,4-biphenyltetracarboxylic dianhydride (BPDA) and *p*-phenylenediamine (PPD) monomers. The formation of PI polymers from the two types of monomers usually involves a two-step process, as illustrated in the lower panel of Fig. 2. First, the diamines and the dianhydrides react to form a poly(amic acid) (PAA) precursor. During this step, the length of the molecular chain is determined, and therefore the average molecular weight of the final PI polymer is dependent on this step. Then, a cyclodehydration reaction takes place, where H_2O is extracted from the structure to form the imide groups. During this step, the PI polymer achieves superior physical and chem-

Table 1
Comparison of physicochemical properties of various polymers for separators.

Polymer	Melting point (°C)	Tensile modulus (GPa)	Coefficient of thermal expansion (ppm/K)	Dielectric constant (1 MHz, 25 °C)	Ref.
Polyimide	>350	3.03	35	3.1–3.5	[31]
Polyethylene	115–135	0.11–0.45	108	2.25	[12]
Polypropylene	150 ~ 165	1.5–2	32	2.1	[12]
Polyvinylidene difluoride	~170	~0.17	80–140	8.4	[32]
Polyacrylonitrile	~300	-	70	4.2	[33]

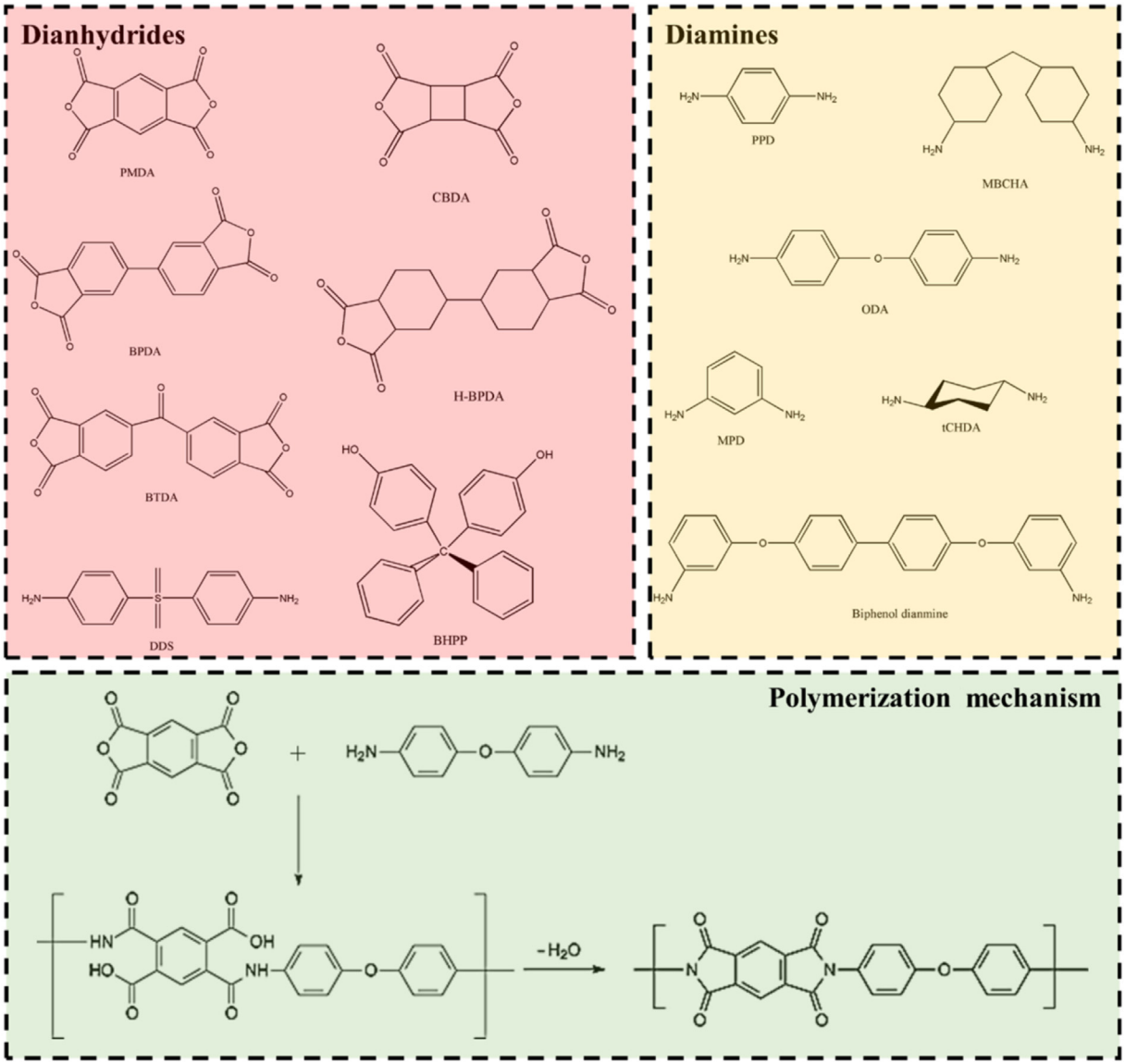

Fig. 2. Typical molecular structures of PI monomers: dianhydrides (left) and diamines (right). The polymerization mechanism of PI from PMDA and ODA monomers (bottom). Cyclobutane-1,2,3,4-tetracarboxylic dianhydride, hydrogenated 3,3′,4,4′-biphenyltetracarboxylic dianhydride, benzophenone-3,3′,4,4′-tetracarboxylic dianhydride, diaminodiphenylsulfone, 4,4′-diaminodicyclohexyl methane, *m*-phenylenediamine, and 1:1,4-cyclohexanediamine are abbreviated as CBDA, H-BPDA, BTDA, DDS, MBCHA, MPD, and tCHDA, respectively.

ical stability. The first PI polymer with high molecular weight was reported in 1955, and its mass production and widespread industrial application started afterward [34]. Detailed physical and thermal features of PI may be exemplified by its most successful commercial product, i.e., Kapton®, produced from PMDA and ODA monomers. Kapton® has good mechanical strength within a wide temperature range, a high glass transition temperature above 360 °C, and a low coefficient of thermal expansion (CTE). These superior features make them good candidates for next-generation LIB separators. It is worthwhile to note that for application as separators in LIBs, many other parameters need to be taken into consideration, in addition to mechanical strength and heat resistance. Properties such as electrochemical stability, electrolyte wettability, and dielectric constant significantly depend on the type of PI used and its corresponding molecular structure. In this section, we briefly describe the classification of PIs, their molecular structures, and some of the most important physical/chemical features.

PIs are most commonly classified based on the structures of the monomers, which determine the physical and chemical properties of the final product. In this context, PIs are classified into fully aromatic PIs, semi-aromatic PIs, and nonaromatic PIs [35]. The aromatic PI molecular chain comprises an electron donor diamine and an electron acceptor dianhydride with a conjugated backbone and high rigidity. Because the superior heat resistance of PIs arises from the transfer interaction from charge transfer complexes, aromatic PIs exhibit better thermal stability because of the enhanced molecular interactions between the conjugated bonds and the rigid molecular chains [35]. Although aromatic PIs are the focus of intense research interest and comprise the largest population in terms of their outstanding thermostability, they also exhibit some disadvantages in specific battery applications. For example, the poor solubility of aromatic PIs in organic solvents leads to high processing costs. The brittleness of the membrane results in low reliability when mechanical strain is applied. The rigid molecular backbone results in low mobility of the Li^+ groups in dry PIs, making them unsuitable for solid polymer electrolytes. As a result, it is often necessary to introduce flexible units into the molecular backbone and tune the overall properties of the PI.

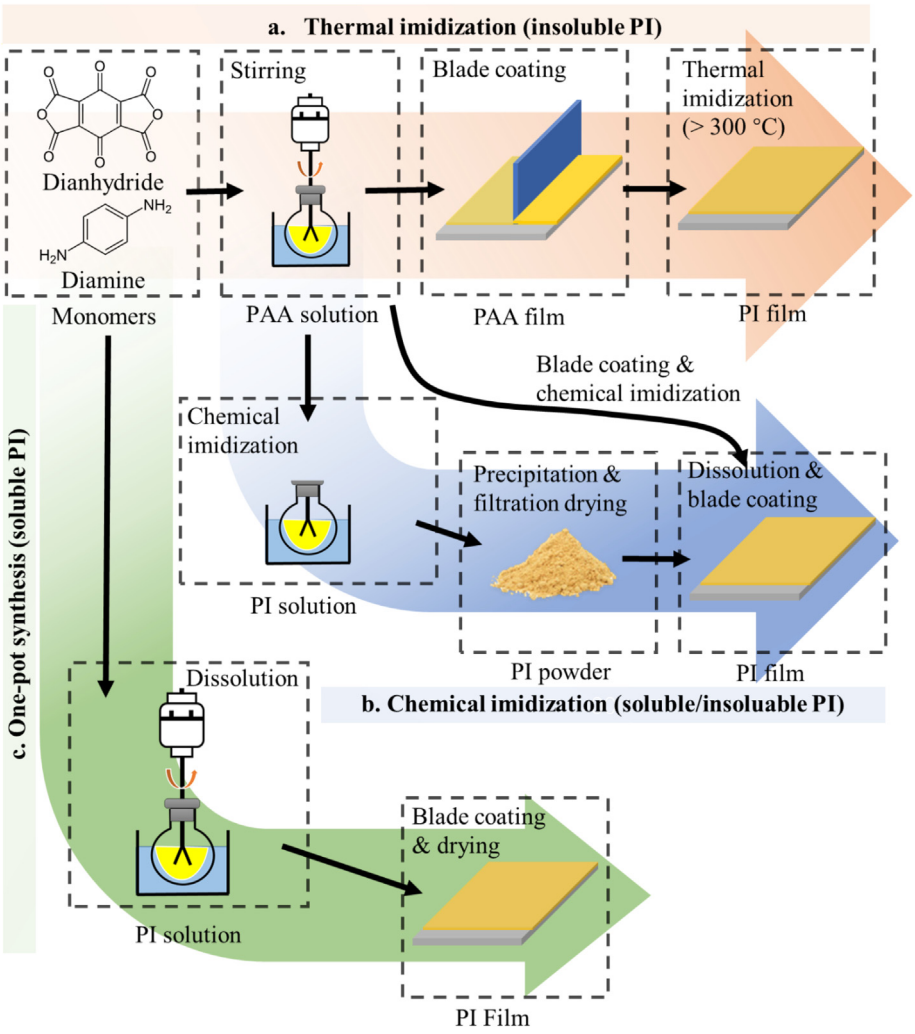

Fig. 3. Illustration of the methods used to prepare porous PI separators.

Nonaromatic PIs contain one or two aliphatic units, and their molecular interactions are not as strong as those of fully aromatic PIs. With alicyclic and aliphatic monomers and fewer molecular interactions, nonaromatic PIs have better optical transparency and better solubility, with tunable thermal stability and mechanical strength. Although optical transparency is not directly related to the separator applications in current commercial LIBs, this type of PI, often called colorless PI (CPI), is becoming an attractive material for next-generation superior plastic applications in optoelectronic engineering. The use of transparent and soluble PIs not only opens new avenues of research on the *in-situ* optical characterization of electrodes but also enables facile processing of PIs as CPIs are soluble in common solvents such as N-methyl-2-pyrrolidone. However, aliphatic PIs suffer from several disadvantages, including the low extent of polymerization with salt formation, brittleness of the film, and poor heat resistance.

Notably, the fabrication method of a PI may strongly depend on the choice of monomers and the corresponding solubility of the final PI product, as illustrated in Fig. 3. In fact, the synthesis route discussed previously (bottom panel of Fig. 2) is usually used for insoluble PIs, where a two-step method is involved, as demonstrated in Fig. 3(a). Monomers are first polymerized to obtain the PAA intermediate, and then the cast PAA film undergoes complete thermal imidization at a relatively high annealing temperature above 300 °C [36]. Apart from thermal imidization, chemical routes are also possible by the addition of dehydrating reagents, as shown in Fig. 3(b). Such chemical imidization processes can be used to synthesize both soluble and insoluble PIs. Apart from these two-step methods, one-pot synthesis has also been developed to fabricate soluble PIs.

3.2. Molecular structure design and properties of PIs

The thermal stability, mechanical properties, CTE, and electrochemical properties of PI films are closely related to the LIB performance. In this subsection, we discuss how to adjust the properties of PIs by designing the structure of the molecular backbone and incorporating segments.

The outstanding thermal stability of PIs is one of the most important reasons that they have been studied as separator materials for LIBs. Thermal stability is usually assessed using the glass transition temperature, T_g, instead of the softening temperature or melting temperature because the transition to the rubbery state increases molecular mobility and impairs the properties of LIB separators. Because the T_g of PIs usually reaches ~ 300 °C, and is thus well beyond the degradation temperature of electrolytes of current LIBs, the thermal stability of PIs is not a major bottleneck for PIs being used as separator materials. In fact, most PIs are far superior to other polymers used in commercial LIBs owing to their thermal

stability, as shown in Table 1. Therefore, while some PIs are less stable than others at elevated temperatures, they are generally able to fulfill the temperature requirements of LIBs. In some special cases where the batteries need to operate at extreme temperatures, enhancing the rigidity of the molecular backbone generally increases the heat resistance of PIs. For example, benzene rings, benzimidazole, benzoxazole, or benzothiazole rings can be included in the structure [6,7]. Some detailed design principles of high-temperature-resistant PIs have been thoroughly discussed in our previous reviews [6,7].

However, fully rigid molecular chains limit the molecular rotation and chain packing, which impair the mechanical strength of PI films and lead to brittleness and cracking of the films. Therefore, a balance has to be achieved between thermal stability and structural flexibility. Thus, PIs modified with specific new monomers, such as asymmetric noncoplanar structures, polar fluorine substitutions, or other thermally stable segments, have achieved some success. Introducing flexible linkages, such as –O–, –CH_2–, and –SO_2– into the rod-like backbone can increase the molecular chain flexibility by decreasing the rigidity of the polymer backbone and inhibiting close packing of the chains. It is worth noting that T_g not only depends on the concentration of these flexible linkages but also on the linkage position and the type of linkage bonds [37]. Linkages in the dianhydride unit affect the T_g value of PIs more than those in the diamine unit.

Apart from the thermal stability and mechanical flexibility, the solubility of PIs can also be tuned. For example, monomers with bulky pendant groups or noncoplanar structures can modify molecular chain packing and molecular interactions and introduce new features such as solubility and high transmittance. Spiral structures, which are characterized by two rings connected by a spiral center, and cardo-structured monomers are typical coplanar units. When Ayala et al. synthesized novel PIs with new dianhydrides containing bulky *t*-butyl and phenyl pendant groups, the products' solubilities greatly improved, and T_g was in the range of 250 ~ 270 °C [38]. Bis(4-hydroxyphenyl) diphenylmethane (BHPP) was reported in the preparation of novel PIs with bulky pedant groups and noncoplanar molecular chains to disrupt chain packing density and enhance tensile strength. Liaw et al. first reported the synthesis of BHPP from the acid-catalyzed condensation of ketones with excess phenol in the presence of hydrogen chloride [39].

The dielectric and optical properties of PIs are also tunable. Novel nonaromatic PIs with cycloaliphatic units have been reported recently in CPI research and low-electric-constant PIs field. Low dielectric materials prevent short circuits, whereas high solubility is good for facile processing [35,40]. Moreover, separators made from colorless or transparent PIs may open new avenues for the optical characterization of electrodes and interfaces in LIBs because the currently used PP or PE separators are nonpermeable to visible light. In general, PIs with electron-withdrawing groups such as trifluoromethyl and sulfonyl groups show lower dielectric constants and high transparencies [31]. Fluorinated PIs (FPIs) were first developed to lower the dielectric constant of PIs to serve as dielectric materials in electronic devices [31]. The small dipole and low polarizability of the C–F bond decrease the dielectric constant and moisture absorption of PIs. This characteristic of FPIs makes them suitable for separator applications in LIBs. Including fluorinated monomers in the structure decreases the dielectric constant, which decreases until the effect saturates [41]. However, FPIs with flexible chains often demonstrate large conformational freedom and high CTE, which might impair the reliability and lifetime of LIBs. The CTE of FPIs can be tuned by increasing the rigidity of the main chains through molecular design and composite co-blending.

4. PI separators for LIBs

As mentioned previously, LIB separators prevent physical contact between the positive and negative electrodes while allowing for Li^+ migration. Because Li^+ transport in LIBs is mediated by the liquid electrolyte, the separators have to contain a significant number of open spaces that percolate throughout the membrane. Therefore, open porous structures need to be created within the PI membranes while maintaining their mechanical integrity. In fact, the microstructures of the membranes are as important as the molecular structures of the PI polymers for application in LIBs. Based on the structures of the pores, PI separators can be classified into two types: porous and fibrous. Porous PI membranes are characterized by connected open pores in a continuous membrane, whereas fibrous membranes comprise an integrated framework of PI fibers. In this section, we introduce these two main types of PI separators, their fabrication processes, and their characteristics.

4.1. Porous PI separators

Porous PI separators are fabricated by creating pores in a continuous membrane. In general, they can be obtained using sacrificial templating, phase inversion, and track-etching, as illustrated in Fig. 3.

4.1.1. PI separators made by sacrificial templates

The sacrificial template method is a widely used technique for creating porous structures in polymer membranes. In this method, porogens are first mixed with a PI or PAA solution, followed by casting the solution into a thin film. The porogens are then removed either by reaction or dissolution from a dried polymeric film, leaving the porous structure in the film. Porous PI separators have been successfully prepared by the sacrificial template method, and so far, different porogens have been applied to create porous structures. Notably, porous structures are determined by the morphologies, concentrations, and packing states of the templates. The removal process of such templates may also play a role in determining the structure of the separator.

A general sacrificial template method using monodispersive templates is shown in Fig. 4. A nanoscaffold-structured PI membrane was reported by Kim et al. using a new one-pot selected etching method with SiO_2 nanoparticles as the porogen in a UV-crosslinked ethoxylated trimethylolpropane triacrylate (ETPTA) polymer matrix integrated with a polyethylene terephthalate (PET) nonwoven substrate [42]. The inverse replica of the hexagonally close-packed SiO_2 nanoparticle superlattices had a periodic three-dimensional (3D) porous structure. As the power density increased, the cells with the reported PI separator exhibited higher energy densities. This novel preparation method can be used to cure PI membranes to obtain flexible and thinner PI separators. A similar approach was adopted by Maeyoshi et al., who fabricated a 3D-ordered macroporous PI separator, which led to the uniform current distribution and enhanced cycle stability of $LiCoPO_4$. In their report, monodispersed silica particles were used as the template to create a 3D-ordered microporous (3DOM) structure. The authors later used this 3DOM PI separator in highly concentrated sulfolane-based electrolytes, hoping to resolve the poor wettability issue in PP separators [43]. The polarity and high porosity of the PI membrane effectively improved the affinity of the separator toward the concentrated electrolytes and allowed for the formation of an anion-derived SEI layer, achieving a long-term stable Li metal anode. In addition to thermal stability and mechanical strength, the uniform porous structure of the 3DOM PI membrane could lead to superior cell performance over PP separators [44]. The effect of the pore size of the 3DOM membrane on lithium

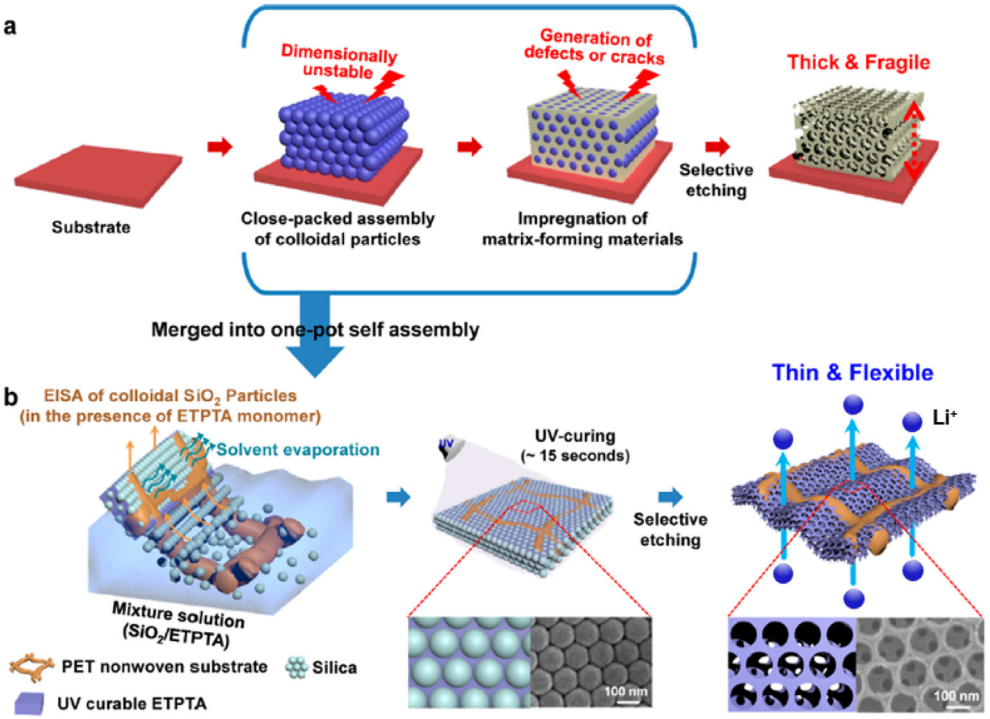

Fig. 4. Schematic representation of the overall fabrication procedure for an inverse opal-mimic nanoporous structure: (a) traditional template approach, (b) separator manufactured via the simple one-pot EISA of SiO_2 nanoparticles in the presence of a UV-curable ETPTA monomer inside a PET nonwoven substrate, followed by UV crosslinking and selective removal of the SiO_2 nanoparticle superlattices [42]. Copyright 2014, American Chemical Society Publications.

deposition and dissolution was explored by the same group [45], where 3DOM membranes with 300-, 500-, and 800-nm pore sizes were tested in Li-Cu cells. The uniform current distribution from the ordered separator pores resulted in uniform Li deposition and dendrite suppression. Ionic conductivity increased with decreasing pore size, and the cells with 300-nm 3DOM achieved the highest cyclability of the Li-metal anode.

In addition to SiO_2, LiBr salt can also serve as a template that can be conveniently removed by dissolving in water, as reported by Lin and coworkers [46]. PMDA and ODA monomers were chosen to obtain the PAA intermediate, and ~ 14 nm fumed SiO_2 nanoparticles were added to the PAA solution to modify the membrane's wettability, thermal stability, and pore morphology. The doctor-bladed PAA membrane was washed with DI water to remove LiBr, followed by an annealing process. With improved thermal, mechanical stability, and electrolyte wettability, the full cell achieved stable cyclic performance over 200 cycles at C3. The integrated PI/Cu/PI separator can also perform dendrite detection in the safety battery design, which will be introduced later.

Apart from inorganic particles, polymers can also be used as porogens. For example, polyether (PEX) is used as a porogen in PAA membranes, as reported by Zhang and coworkers [47]. The as-prepared PI separator showed sponge-like pores with high porosity. Furthermore, the PEX concentration of 40 wt% was reported to show an optimal ionic conductivity of 2.15×10^{-3} S cm^{-1} and an improved discharge capacity of 62.4 mAh g^{-1} at 4.0 °C compared to the PP separator. The abovementioned studies used a single porogen to produce a porous structure. Li et al. took this a step further and reported a new PI prepared with two porogens: dibutyl phthalate and glycerin, which showed better tunability and microstructural control [48]. The as-obtained separators showed higher porosity and a more uniform pore-size distribution than the separators prepared with a single porogen. The as-prepared PI separators exhibited great thermal stability and enhanced ionic conductivity, and the coin cells assembled with the PI separator operated steadily after heating at 140 °C for 1 h.

In general, the sacrificial templating method can generate PI separators with excellent properties that fulfill the requirements of LIBs. This method is also compatible with the current industrial polymer film fabrication process involving roll-to-roll casting followed by solvent evaporation. However, this method involves an additional template removal process. Such a process may lead not only to additional processing costs but also to potential safety hazards. For example, when SiO_2 is used as the templating agent, highly hazardous hydrofluoric acid needs to be incorporated to remove it. In this regard, reusable, environmentally friendly, and low-cost templates need to be developed.

4.1.2. PI separators made by nonsolvent-induced phase separation method

The nonsolvent-induced phase separation process (NIPS), also called the phase inversion process, can also be used to prepare porous polymeric membranes. This method has been successfully used to produce ultrafiltration and microfiltration membranes, gas separation membranes, ion exchange membranes, etc. [49]. In NIPS, a polymer solution is first cast into a thin film, which is then immersed in a coagulation bath containing a nonsolvent. In the solvent–nonsolvent–polymer ternary phase system, as the nonsolvent exchanges with the solvent, the polymer will precipitate to create porous structures. In this process, the porous structure created by phase inversion can be controlled by tuning the composition and aging time of the antisolvent bath. Wang et al. first adopted NIPS to prepare porous PI membranes from a blade-cast organosoluble PI resin [50]. In their study, 1,4-bis(4-amino-2-trifluoromethylphenoxy)benzene (6FAPB) and ODA were chosen as the diamines and 3,3′,4,4′-diphenylsulfone tetracarboxylic dianhydride (DSDA) as the dianhydride. The solubility of this aromatic PI is attributed to the bulky trifluoromethyl groups in the molecular backbone and the disordered molecular structure of copolymer-

ization, which disrupts the dense chain stacking. The prepared polyimide resin was dissolved in dimethylacetamide (DMAc), and ethanol/DMAc was used as a nonsolvent coagulation bath to obtain porous PI membranes. Different coagulation bath compositions and solids contents of the PIs were investigated. It was found that a large amount of ethanol could effectively precipitate PI, and the obtained separator had a sponge-like structure. The final membrane possessed a tensile modulus comparable to that of commercial Celgard®2400 in the transverse direction, an enhanced T_g at 274 °C, and good wettability toward electrolytes. With large porosity, these membranes showed increased electrolyte uptake from 190% to 379%, higher ionic conductivity than a Celgard®2400 membrane, and flatter voltage plateaus in the discharge curves for the Li-ion cells.

During NIPS, the surface chemical properties may be altered according to the baths being used. Such surface features can significantly affect the wetting behavior of the electrolyte and thus the Li^+-ion transport. Therefore, post-processing is sometimes necessary to obtain the desired properties for PI separators fabricated using the NIPS method. It was reported that through alkaline hydrolysis by immersing the PI separator in a NaOH bath, the PI separator made from the NIPS can be modified with the –COOH group [51]. The Li^+ transport rate on the surface of the PI–COOH separator was calculated to be more than six times higher than that of the original PI separator, and the cell showed improved cycle performance and rate capability.

To briefly summarize, although the NIPS method is a promising method that does not require additional removal of templates, the quality of the separators strongly depends on the processing parameters. Sometimes these parameters can be difficult to control precisely, such as the immersion time and the concentration of different contents of the bath. Therefore, the industrial application of NIPS to fabricate PI-based separators may need additional exploration to reduce the sensitivity of the structural features of the final product toward the processing parameters.

4.1.3. PI separators made by track-etching

The track-etching technique is a frequently used industrial technology that produces membranes. The track-etching effect of thin films was first discovered by Fleischer in 1964 when preparing a novel filter for biological materials [38]. During the track-etching process, heavy ions such as uranium track swiftly across thin film surface to create vertically aligned tracks across the film's cross-section, providing highly homogeneous tracks and precise control of the track size and density. A PI separator with aligned channels was prepared through the track-etching technique and applied with a solid polymer composite electrolyte in an LIB [52]. Because the membrane is used as a solid electrolyte (SE) in an SSB, the details will be discussed in Section 6.3. Briefly, the separator is made of a PI host with vertically aligned nanochannels infused with other polymer electrolytes. The high-modulus host prevents potential dendrite penetration, and the aligned channels enhance the ionic conductivity. The as-prepared separator is ultrathin, nonflammable, and mechanically strong, preventing short-circuiting after more than 1000 cycles. Because this method requires high-energy ion beams and high vacuum during fabrication, it is more suitable for research purposes instead of mass production.

4.1.4. PI separators made by electrospinning

Fibrous PI separators are another family of porous membranes that are used in LIB applications. Unlike the porous structures mentioned in the previous section, fibrous membranes are fabricated by assembling PI fibers. Usually, fibrous PI separators are characterized by large porosity and therefore provide good ionic conductivity. Usually, fibrous PI separators are fabricated using the electrospinning technique.

4.1.5. Setups and fundamentals of electrospinning

The electrospinning technique is a facile fabrication method for fabricating nonwoven fibers, and it has attracted intensive research interest since the 1990 s [8]. The spinning device typically consists of a syringe pump to control the flow rate of the polymer solution, a spinneret for ejecting fibers, a collector for collecting fibers, and a high-voltage supply to generate an electric current between the spinneret and the collector (Fig. 5a) [53,54]. A uniform polymer solution is prepared before electrospinning. During electrospinning, the polymer solution is charged under a high voltage, resulting in a strong electrostatic force. The balance between the electrostatic force and surface tension transforms the hemispherical surface contour of the solution into a conical shape, called a "Taylor cone" (Fig. 5a). At a critical voltage, the electrostatic force overcomes the surface tension, and a jet erupts from the spinneret. After ejection, the strength of the electrostatic repulsion between the charged jets increases because of the evaporation of the solvent, which splits the jet into several tiny jets. When the jets arrive at the collector, they solidify into nanofibers. Electrospun nanofiber mats have many advantages, such as large surface area, high porosity, tunable morphologies and structures, good mechanical strength, and ease of processing, and thus they are used numerous applications, including filtration, separation, energy storage/conversion, and biomedical engineering [54,55].

In 1996, Reneker et al. first reported the fabrication of PI fibers by electrospinning [56]. However, they did not provide enough information about the processing conditions. Because most PIs are insoluble in organic solvents, the electrospinning of PI fibers usually involves two steps: (1) electrospinning of PAA nanofibers from their solutions and (2) imidization of PAA nanofibers into PI nanofibers. Most PI-based electrospun nanofibers use PMDA–ODA-type precursors. In this section, we review the preparation, characteristics, and electrochemical performance of fibrous PI-based LIB separators.

4.1.6. Homo-PI nanofibers

Homo-PI nanofibers can be readily fabricated by electrospinning the PAA solution followed by imidization, as illustrated in Fig. 5(b). Specifically, the pristine PAA solution is synthesized via the polymerization of one dianhydride (e.g., PMDA) and one diamine (ODA) with an equivalent molar ratio. Subsequently, the PAA solution is used for electrospinning, obtaining PAA nanofibers. Finally, the PAA nanofibers are converted into PI nanofibers upon thermal imidization in a temperature range of 250–450 °C depending on the fibers' molecular structures. Miao et al. first adopted PMDA and ODA monomers to prepare the PAA precursor solution [57]. The scanning electron microscope (SEM) image in Fig. 5(c) shows that the PI nanofibers had a uniform diameter of ~ 200 nm without any beads. The thermogravimetric analysis (TGA) and hot oven tests revealed that the PI nanofiber-based nonwovens had better thermal stability than the commercial Celgard® membrane. The onset temperature of the degradation of PI nonwoven was over 500 °C, whereas the Celgard® membrane exhibited great shrinkage at 150 °C and it melted above 167 °C. The polarity of PI is similar to that of the organic liquid electrolyte, thereby leading to excellent electrolyte wettability and high uptake of the electrolyte of the PI nanofiber mats. Electrochemical tests showed that the battery using a PI nonwoven separator had a higher capacity, lower resistance, and higher rate capability than the one using the Celgard® membrane (Fig. 5d). To improve the mechanical strength, Jiang et al. mechanically pressed PI nonwoven mats at 1, 2, 3, and 5 MPa for 3 min [58]. When the pressure was increased from 1 to 5 MPa, the tensile strength of the PI nonwovens increased from 12 to 31 MPa with a deformation of ~ 30%. Moreover, the LiBOB/PC-soaked PI nonwovens possessed a high oxidative potential above 4.5 V and an ionic conductivity of

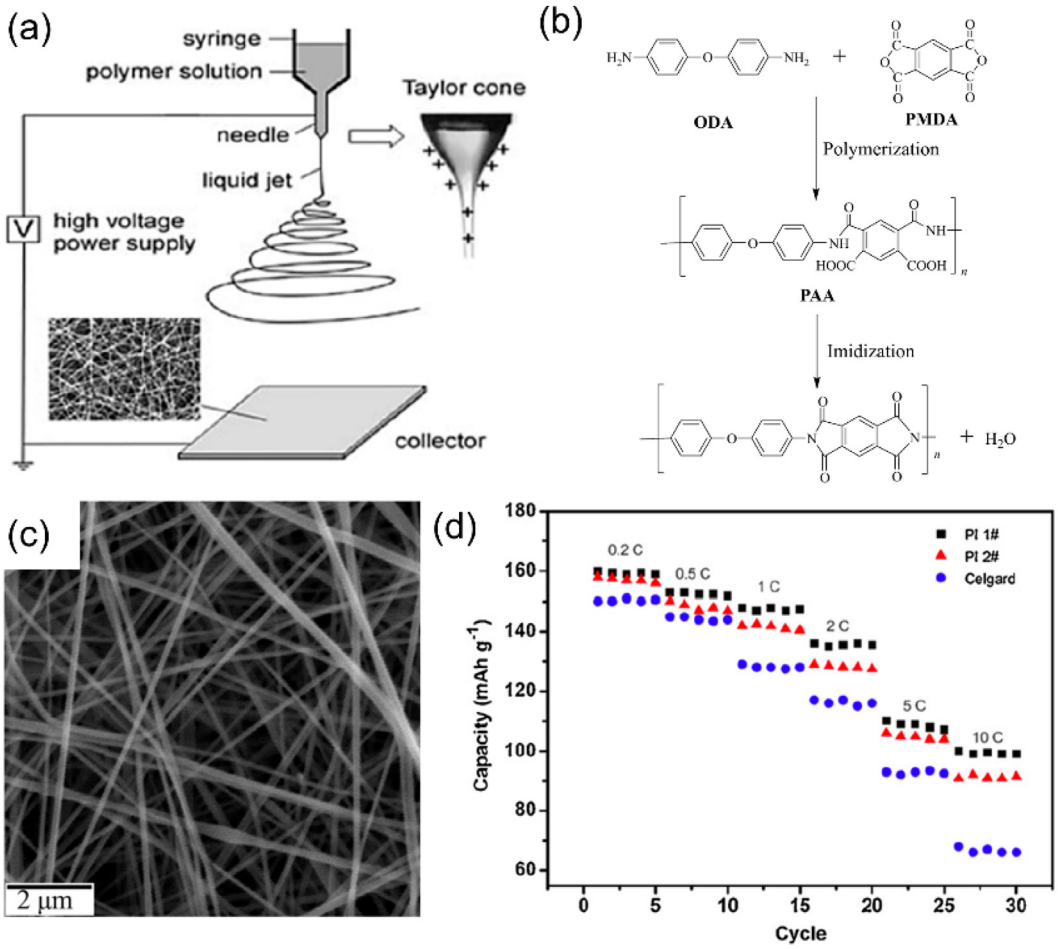

Fig. 5. (a) Schematic of the basic setup for electrospinning. Reproduced with permission [54]. Copyright 2004, Wiley-VCH Publications. (b) Chemical schemes showing the two-step method for synthesis of PMDA–ODA PI. Reproduced with permission [8]. Copyright 2016, Elsevier Publications. (c) SEM image of PI No. 1 nanofiber and (d) rate capability tests for the cells with Celgard® membrane, PI No. 1, and PI No. 2 nanofiber nonwovens as separators. Reproduced with permission [57]. Copyright 2013, Elsevier Publications.

1.73 mS cm^{-1} at 120 °C. As a result, the batteries assembled with PI nonwoven separators exhibited stable charge–discharge profiles and satisfactory cyclability (86% capacity retention after 50 cycles) at 120 °C, showing great promise as a safe LIB separator. Hou et al. reported that hot-press treatment can shorten the imidization time to within 30 min compared to several hours in conventional thermal imidization [59]. The tensile strength of hot-pressed PI was much higher than that of thermal-treated PI without hot pressing, which can be attributed to the increased crystallinity of macromolecular structure and uniform arrangement of the nanofibers.

Making crosslinked PI nanofibers is another strategy to improve their mechanical strength. Kong et al. prepared a crosslinked PI nanofiber membrane via ammonia pretreatment of the electrospun PAA precursor followed by imidization [60]. The loose and weak PI nonwoven was converted into a compact and robust fabric membrane, which was attributed to ammonia-induced crosslinking. The crosslinked PI nanofiber mats had a greater tensile strength (37.5 MPa vs. 10.8 MPa) and a higher onset deformation temperature (380 °C vs. 328 °C) than the noncrosslinked counterparts shown in Fig. 6(a) and (b). The SEM characterization also indicated that the nanofibers were welded together after crosslinking, which reduced the risk of segregating a robust fabric membrane into loose nonwovens during long-term battery cycling, thus improving the integrity of the PI nanofiber membrane as a separator (Fig. 6c–e). The cell assembled with the crosslinked PI nanofiber separator displayed outstanding cyclic stability with 80% capacity retention at 5C (130 mAh g^{-1}), and it operated steadily at 120 °C without any capacity fading. Even though PIs are generally insoluble in common solvents, some organosoluble PIs were synthesized for fabricating electrospun PI nanofibers [23]. Organosoluble PIs are typically synthesized using a solution imidization method. After that, the obtained PIs are dissolved in dimethylformamide or DMAc, and the resulting solution is used for electrospinning. Byun and coworkers prepared organosoluble PI by simple solution imidization between PAA and *o*-xylene [61]. A stable PI nanofibrous membrane was then obtained by electrospinning and thermal crosslinking. When used as a separator, the cell showed significantly improved rate capability, with 80% and 36% capacity retention at 10C and 20C, respectively. By contrast, the battery using the PP separator maintained only 33% and 8.5% capacity under the same conditions. Nevertheless, the tensile strength of the PI membrane was only 6 MPa, which was relatively low compared to that of most electrospun PI nanofibers. Kong et al. prepared a robust FPI nanofiber membrane by an electrospinning technique and a subsequent thermocrosslinking process [62]. The FPI was synthesized from the polycondensation of 6FAPB and dianhydride (ODPA) in an equimolar ratio, as shown in Fig. 6(f). Fig. 6(g) shows the SEM image of the FPI nanofibers. It can be seen that the FPI nanofibers had a diameter of ~ 400 nm and were well crosslinked after imidization. The high fluorine content in FPI nanofiber membranes enhances the flame resistance of the PI and provides greater affinity with the polar liquid electrolyte compared to non-

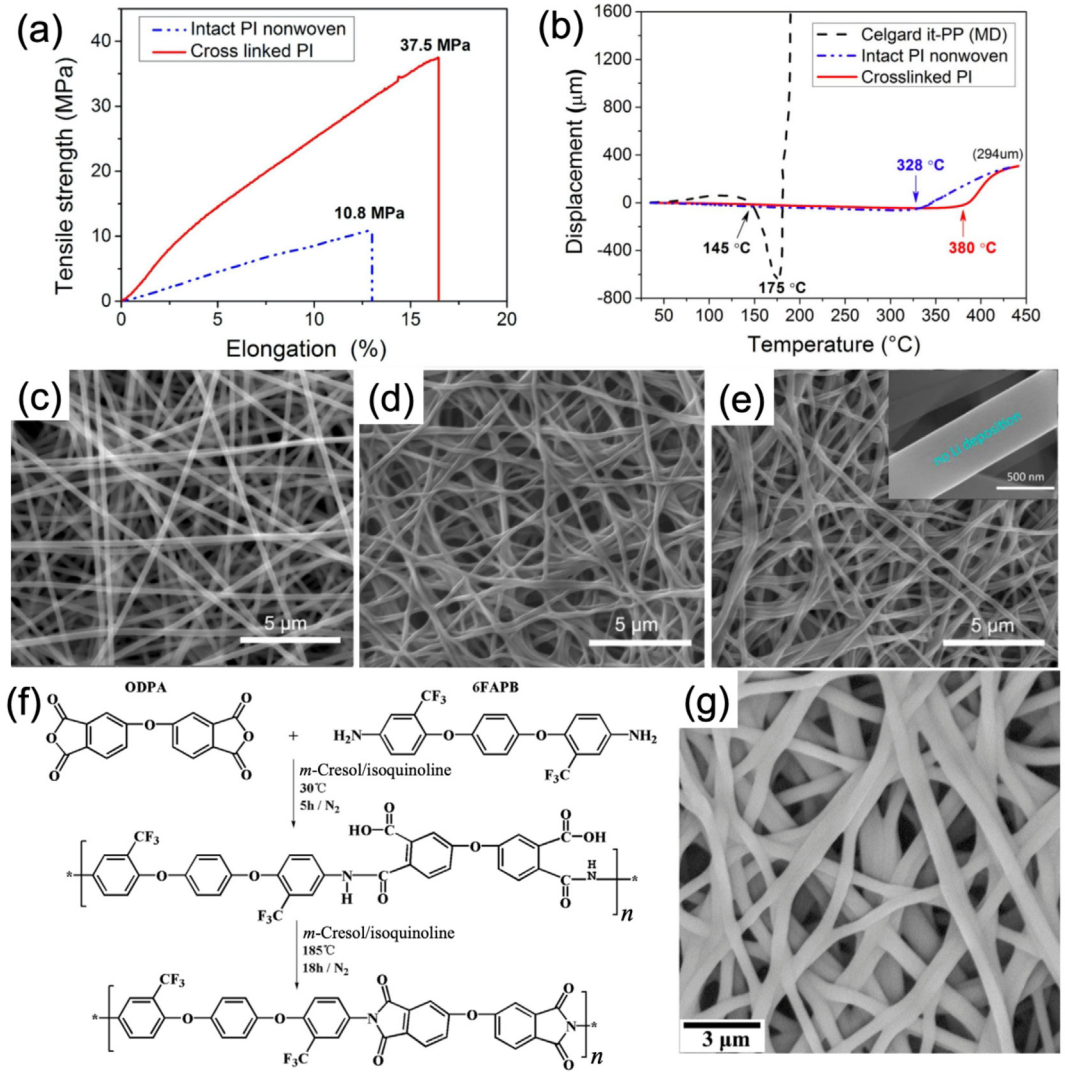

Fig. 6. (a) Stress–strain curves of an intact PI nanofiber nonwoven and a crosslinked PI nanofiber membrane. (b) Thermal mechanical analysis (TMA) curves of a Celgard® it-PP separator, an intact PI nanofiber nonwoven, and a crosslinked PI nanofiber membrane measured under N_2 at 5 °C min^{-1} and 0.2 N loading. SEM images of (c) an intact PI nanofiber nonwoven and (d) a crosslinked PI nanofiber membrane fabricated via the ammonia-induced welding process. (e) Crosslinked PI membrane after 100 charge–discharge cycles in a $LiFePO_4$||separator||Li half-cell; the magnified image is shown in the inset, indicating no Li deposition on the PI membrane. Reproduced with permission [60]. Copyright 2017, IOP Publishing. (f) Schematic of synthesis route and (g) SEM image of FPI. Reproduced with permission [62]. Copyright 2018, Elsevier Publications.

fluorinated membranes and commercial PE separators. Batteries assembled with FPI nanofibers separator deliver higher capacities, especially at high rates, than those using PE separators because of the higher ionic conductivity and lower interfacial resistance of the assembled coin cells. Recently, P-containing PI composite fibrous nonwovens were also designed to improve the mechanical and thermal stabilities of PIs [63].

4.1.7. Co-PI nanofibers

The molecular structure of PIs can be elaborately designed because of the numerous dianhydride and diamide monomers. When the types of dianhydride and/or diamide are equal to or greater than two, the resulting copolymers are called co-PIs. Fig. 7(a) shows a scheme for making a BPDA–PPD–ODA co-PI from one dianhydride monomer of BPDA and two diamine monomers of PPD and ODA each [64]. Similar to homo-PIs, electrospun nanofibers of BPDA–BPA–ODA co-PI can be prepared via a two-step method. The BPDA–BPA–ODA co-PI nanofibers possess very high mechanical strength (i.e., a tensile strength of 1.1 ± 0.1 GPa and an elastic modulus of 6.2 ± 0.7 GPa), reflecting the synergistic effect of the two different (i.e., rigid and rod-like, and flexible) components. Recently, Li et al. fabricated a co-PI nanofibrous mat using a blow-spinning method [65]. Analogous to electrospinning, blow spinning produces nanofibers from polymers dissolved in suitable solvents. As shown in Fig. 7(b), the polymer solution streams are attenuated to ultrafine jets by a high-speed jet stream and solidified into nanofibers on the target. The as-prepared PI membrane (Fig. 7c) possessed satisfactory porosity (87.3%), excellent thermal stability (no shrinkage even up to 180 °C), good electrolyte wettability, and high ionic conductivity (1.74 mS cm^{-1}). The $LiCoO_2$||PI separator||Li possessed a more stable cycling profile and a higher discharge capacity (114.3 mAh g^{-1}) after 100 cycles as compared with the Celgard® separator (Fig. 7d).

In summary, compared with porous PI separators fabricated by sacrificial templating, phase inversion, and track-etching methods, the electrospinning technique can produce PI fiber membranes with high porosity, high specific surface area, and controllable pore size. Therefore, electrospun PI-based fibrous membranes are promising candidates for separators because of their appealing fea-

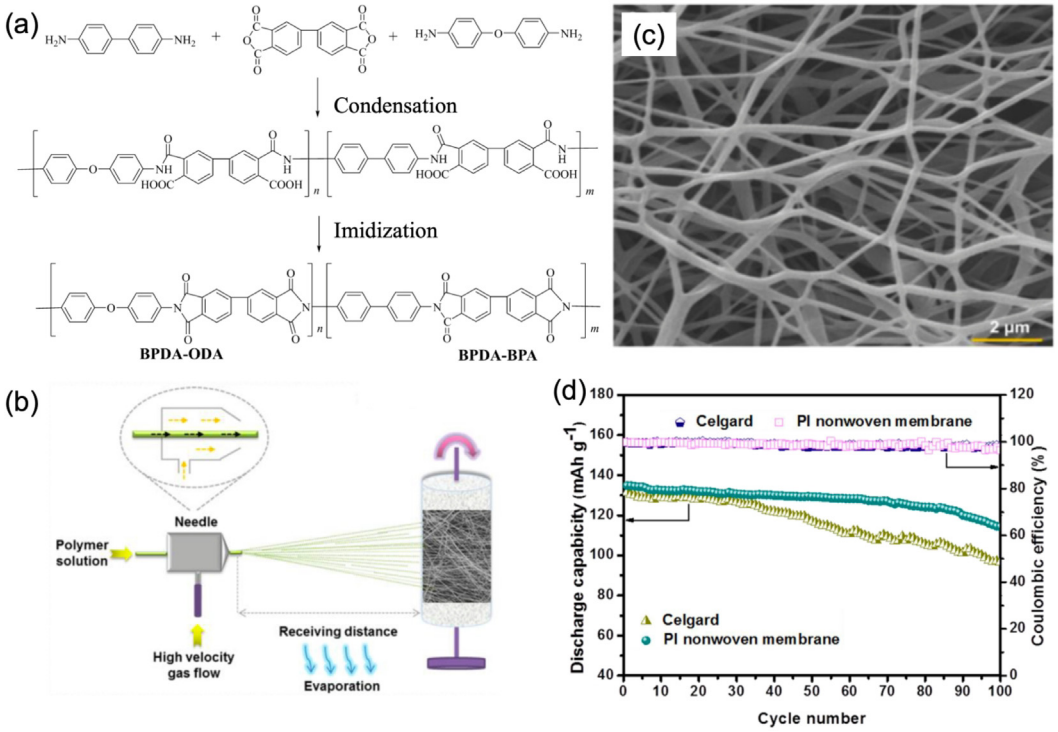

Fig. 7. (a) Synthesis of BPDA–BPA–ODA Co-PI. Reproduced with permission [64]. Copyright 2007, IOP Publishing. (b) Preparation process of the PI nonwoven membrane via solution blow spinning. (c) SEM image of PI nonwoven membrane. (d) Cyclic stability of $LiCoO_2$||Li cells using Celgard® and PI nonwoven membrane separators. Reproduced with permission [65]. Copyright 2018, American Chemical Society.

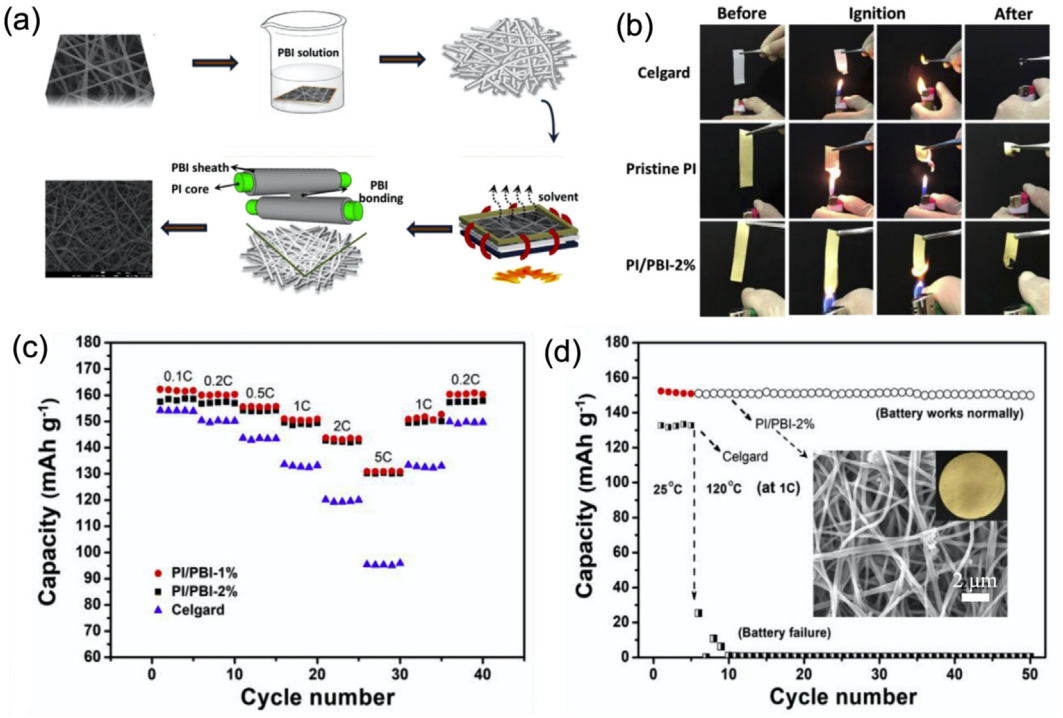

Fig. 8. (a) The mechanism of preparing a PI@PBI-reinforced nanofibrous membrane by a self-compression and self-bonding technique. (b) Combustion tests of the Celgard®, pristine PI, and PI/PBI-2% membranes. (c) Rate capability of $LiFePO_4$||Li batteries using PI/PBI-1%, PI/PBI-2%, and Celgard® membranes. (d) Cycling performance of $LiFePO_4$||Li batteries at a high current density of 1C at 25 °C and 120 °C. The insert shows the SEM and optical images of the PI/PBI-2% membrane at 120 °C. Reproduced with permission [77]. Copyright 2019, Elsevier Publications.

tures such as interconnected pore structures, high porosities (up to approximately 90%), large surface-to-volume ratio, and good tunability, all of which contribute to fast ion conduction, which is essential for high-performance rechargeable batteries [66,67].

5. PI-based composite separators for LIBs

Excellent mechanical properties, high porosity, good wettability, and superior thermal stability make PIs suitable as high-performance separators. As mentioned in Section 3, PI membranes for use as separators can be fabricated by diverse methods, including electrospinning, phase conversion, and templating. However, the fabrication cost of PIs is higher than that of polyolefins, and their mechanical properties are worse than those of the latter. Therefore, PIs are often hybridized with other materials such as polyolefins and ceramics to further improve their mechanical properties and wettability. In general, such PIs can be classified into PI-modified and PI-support composite separators. In the following section, we discuss the fabrication of PI composite separators and their characteristics.

5.1. PI-based composite separators for LIBs

To mitigate the thermal shrinkage of conventional polyolefin-based separators, PI is incorporated to improve their overall thermal properties [68,69]. For example, PI aerogel particles were first mixed with PVDF in an N-methyl-2-pyrrolidone (NMP) solution and then coated on one side of the PE separator by casting [69]. When both PE and PI-modified PE separators were heated at 140 °C for 30 min, the PI-modified PE separator showed 0% thermal shrinkage, whereas the PE separator showed 50% shrinkage. To further improve the thermal stability, Al_2O_3/PI composite surface coatings were applied to PP separators [70]. The Al_2O_3/PI-coated PP separators remarkably suppressed internal short circuiting. In another study, PI/PET-layered composite separators were prepared using PET nonwovens as supports to collect electrospun PI nanofibers [71]. The highly porous PI nanofiber mats increased the uptake of electrolyte, whereas the PET component contributed to the high tensile strength of the composite separators. Moreover, the PI/PET-layered composite separators exhibited a thermal shrinkage of only ~ 2% at 180 °C. The Li-ion cells using the PI/PET composite membrane showed stable cyclic performance and better rate capabilities than the cells using Celgard® separators. PI has also been used to modify glass fiber membranes. For example, Zhang et al. applied a PI coating to a glass fiber (GF) membrane through a simple dip-coating method [72]. The PI component filled the pores among the fibers, enhancing the connection between neighboring fibers. After incorporating 20 wt% PI, the tensile strength of the GF increased from 1.1 to 23.8 MPa. In addition, the cycle performance at 120 °C demonstrated that the GF/PI composite membrane could serve as a safe and high-power LIB separator.

5.2. PI-supported composite separators

5.2.1. PI/polymer composites

In addition to incorporating the PI component into different matrices, PI itself can be fabricated as a freestanding matrix to form a composite with other materials. To date, various PI nanofiber mats have been fabricated by the electrospinning technique [73]. Because PI nonwovens are usually prepared with rather low mechanical properties because of the weak interaction between PI fibers, polymers with low melting temperatures are incorporated to fuse nanofibers and therefore enhance the separator's tensile strength [74]. Liang et al. developed a polyethylene oxide (PEO)-coated electrospun PI fibrous separator by an electrospinning method followed by a dip-coating and drying process [75]. The $LiFePO_4$||Li battery with a PEO-coated PI separator showed an excellent rate capability (80 mAh g^{-1} at 5C) at 0 °C, which was much higher than that of the cell with a PP separator. Similarly, Hsieh and coworkers introduced PE into PI mats (PE@PI) by simple spin coating [76]. The as-obtained PE@PI film without any shrinkage at 150 °C exhibited high porosity (80%), high electrolyte uptake (1350%), and good ionic conductivity (1.2×10^{-3} S cm^{-1}). PI-core@polybenzimidazole-sheath (PI@PBI) nanofibers were proposed as an ultrahigh-strength, nonflammable, and high-wettability separator for advanced LIBs [77]. The fabrication process of the PI@PBI separator is illustrated in Fig. 8(a). The as-synthesized fibrous membrane possessed an ultrahigh strength of 59 MPa and super-high thermal dimensional stability at 300 °C. The unique fire resistance of PBI also ensured the high security of batteries (Fig. 8b). Notably, the battery using the PI@PBI separator displayed a much higher capability (130.2 mAh g^{-1} at 5C) than the battery with the Celgard® separator (95.4 mAh g^{-1} at 5C), as shown in Fig. 8(c). More impressively, the battery assembled with the PI@PBI separator could work steadily at 120 °C and maintain outstanding cyclic stability owing to the superior thermal stability of the PI@PBI membrane (Fig. 8d).

Cai and coworkers reported the fabrication of a side-by-side thermoplastic polyurethane (TPU)/PI membrane, where the integrated thermally stable PI and highly elastic TPU showed a synergetic effect [78]. The fluorescence microscopy image of the TPU/PI fibers showed that green TPU and orange PI were observed in one fiber, and there was a clear interface between the different components. The TPU/PI mats had a high tensile strength of 8.85 MPa, which was ~ 50% higher than that of the pure TPU mats. This phenomenon can be explained by the formation of a transition layer between the two components. Apart from outstanding mechanical properties, . Even at 230 °C, the TPU/PI membrane showed no dimensional change thanks to the existence of PI. In addition to TPU, PVDF has also been hybridized with PI [79]. Park *et al.* made a multicoreshell PI-reinforced PVDF nanofiber for an LIB separators using simple electrospinning of one type of solution with two immiscible polymers [79]. The structure of the single fiber could be easily tuned by controlling the weight ratio of PI to PVDF. The unique PI-reinforced PVDF separator showed better thermal stability, mechanical properties, and long-term battery performance than a commercial PE separator. Research has also been devoted to preparing electrospun PI composite nanofibers with other polymers such as poly(vinylidene fluoride-co-hexafluoropropylene) (PVDF-HFP) [80–82]. In 2012, Liu et al. prepared core–sheath PI@PVDF-HFP composite nanofiber mats/membranes via a coaxial electrospinning method [82]. The PI core material provided superior thermal and mechanical properties, whereas the PVDF-HFP sheath material improved the ion conductivity.

Shutdown behavior is also essential because electrical overcharging and high thermal impact may occur during battery operation. Thus, short circuits would cause TR of LIBs, which could eventually lead to a fire or explosion of the cells. Therefore, a shutdown separator plays a crucial role in separating the electrodes and/or stopping the electrochemical reactions. To mitigate the potential risks, a multilayer polyolefin such as PP/PE/PP, Celgard® 2340, was proposed as a fail-safe device in commercial cells [83]. As shown in Fig. 9(a), a low-melting-point PE was sandwiched between the two PP membranes and acted as the shutdown agent. When the temperature was higher than the melting temperature of PE (~130 °C), the PE layer collapsed and blocked the ion conduction. However, when the temperature continuously increased above the melting point of PP (~160 °C), the PP layers started to shrink and the separator failed to separate the electrodes, causing internal shorting of the cell. Considering the excellent thermal properties of PI, the shutdown behavior of PI nanofibers can be achieved by modifying them with low-melting-point polymers such as PE [83], PEO [75], PVDF [84], and polyetherimide (PEI) [22]. For example, Shi et al. coated a layer of PE microparticles onto electrospun PI nanofibers [83]. In 2015, Wu et al. first reported a

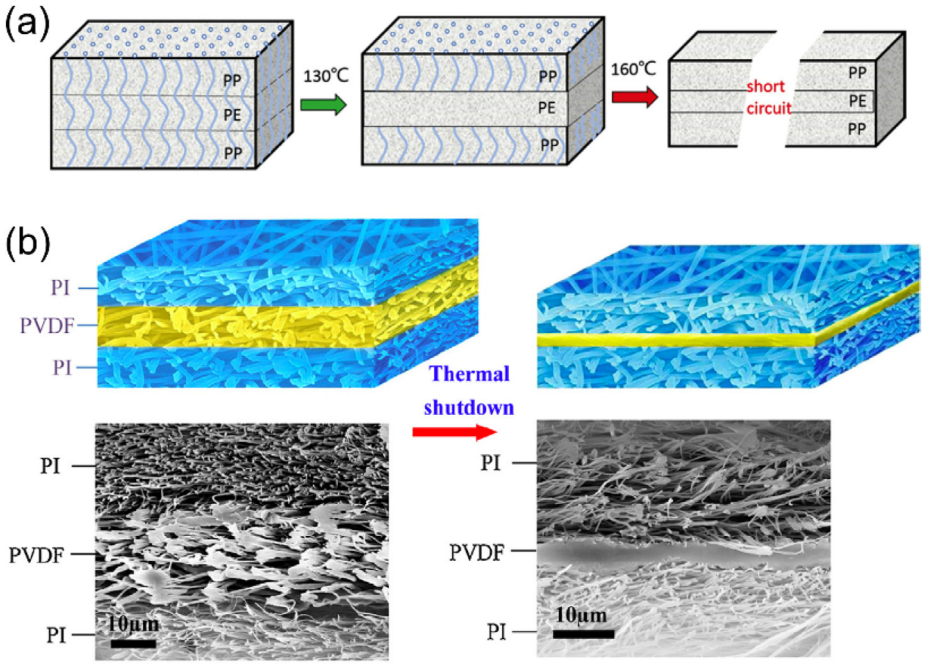

Fig. 9. (a) Shutdown behavior of PP/PE/PP separator. Reproduced with permission [83]. Copyright 2015, Elsevier Publications. (b) Illustration of the shutdown behavior of the sandwiched PI/PVDF/PI nanofiber separator. Reproduced with permission [84]. Copyright 2015, Elsevier Publications.

sandwiched PI/PVDF/PI composited nanofiber separator [84]. A middle layer of PVDF nanofibers was sandwiched between two PI nanofiber mats, a structure similar to that of the conventional PP/PE/PP separator. When the battery was heated at 170 °C, the PVDF nanofibers melted and formed a pore-free film, thus shutting down battery operation (Fig. 9b). Recently, Sun et al. proposed a new and practical tri-layer separator through an *in-situ* welding process in which PBI sheath@PI core nanofiber mats were used as the structural support and melt-processable PEI nonwoven was used as the interlayer [22]. The *in-situ* welding technique is simple and controllable, and it can integrate the comprehensive functions of PBI, PI, and PEI, making it promising for low-cost industrial production. Compared to the PI/PVDF/PI separator, the PBI@PI/PEI/PBI@PI (PBEI) separator had a high shutdown temperature of approximately 235 °C. In addition, PEI is a good flame retardant. Therefore, the unique flame retardancy of the PBEI separator, in combination with its shutdown function, is expected to ensure the safety of LIBs.

5.2.2. PI/ceramic composites

Inorganic fillers such as metal oxides have been widely used to enhance the wettability and mechanical properties of separators. For example, Al_2O_3 nanoparticles are commonly used to coat polyolefin separators through a wet coating procedure [85]. With a thin Al_2O_3 layer, the thermal stability and electrochemical performance of PE separators can be significantly improved [85]. The hybridization of inorganic components with PI has also been well investigated [86–88]. Electrospun PI/ceramic composite nanofibers can be obtained either by electrospinning a mixture of PAA and other components (e.g., inorganic particles and their precursors) or by adopting post-treatment and/or surface modification of PI nanofibers after electrospinning.

Direct mixing before electrospinning. It is straightforward to make electrospun composite nanofibers by directly dispersing nanoscale fillers in spin dope. Many PI composite nanofibers have been prepared by directly adding nanofillers or precursors into PAA solutions for electrospinning followed by thermal imidization [89,90]. Cheng et al. reported the fabrication of PI/silica hybrid nanofibrous mats/fabrics by combining electrospinning and *in-situ* sol–gel synthesis [91]. Specifically, tetraethoxysilane (TEOS) was first added to a PAA (PMDA–ODA) solution, which was then electrospun into nanofibers. After treatment, PI nanofibers containing silica nanoparticles were obtained. With 6.58 wt% SiO_2 in the PI/SiO_2 hybrid fibers, the decomposition temperature increased by more than 130 °C and the tensile strength was four times higher than that of the neat PI fabric. The above results indicate that the introduction of inorganic fillers can significantly improve the thermal stability and mechanical properties of PI fibers. Wang et al. fabricated a nanosilica-modified PI nanofiber separator by adding nanosilica particles (~15 nm) to a PAA (PMDA–ODA) solution [92]. The obtained PI–SiO_2 composite separator showed excellent electrolyte wettability and large electrolyte uptake (about 2400%), and the $LiMn_2O_4$||Li cell with the PI–SiO_2 separator exhibited highly improved rate capability and cycling stability at 55 °C. In addition to metal oxides, graphene oxide has also been incorporated to improve the porosity, electrolyte absorption rate, and ionic conductivity of the fiber membrane [90,93]. Consequently, the electrochemical performance of the GO/PI film was much better than that of the pure PI membrane.

Post-treatment after electrospinning. Post-treatment and/or surface modification of electrospun PI nanofibers is another common approach to prepare hierarchically structured composite nanofibers. Typically, inorganic nanoparticles are decorated onto the surfaces of nanofibers via physical/chemical interactions. In 2014, a sandwiched Al_2O_3-coated PI nanofiber mat was reported as an LIB separator [94]. First, the PI nanofiber mats were prepared by the electrospinning method. Al_2O_3 nanoparticles were then coated onto the PI nanofiber mats by dip-coating. As shown in Fig. 10(a and b), thin Al_2O_3 layers were coated on both sides of the PI mats. Compared to neat PI nanofiber separators, the Al_2O_3-coated PI nanofiber separators exhibited enhanced capacity, rate capability (78.91% at 10C), and cyclability (95.53% retention after 200 cycles at 1C). Liang et al. also reported the preparation of Al_2O_3/SiO_2–PI composite nanofiber mats by dip-coating Al_2O_3 and SiO_2 nanoparticles on both sides of electrospun PI mats [86]. Recently, thin TiO_2 nanolayers were built on the surface of PI fibers

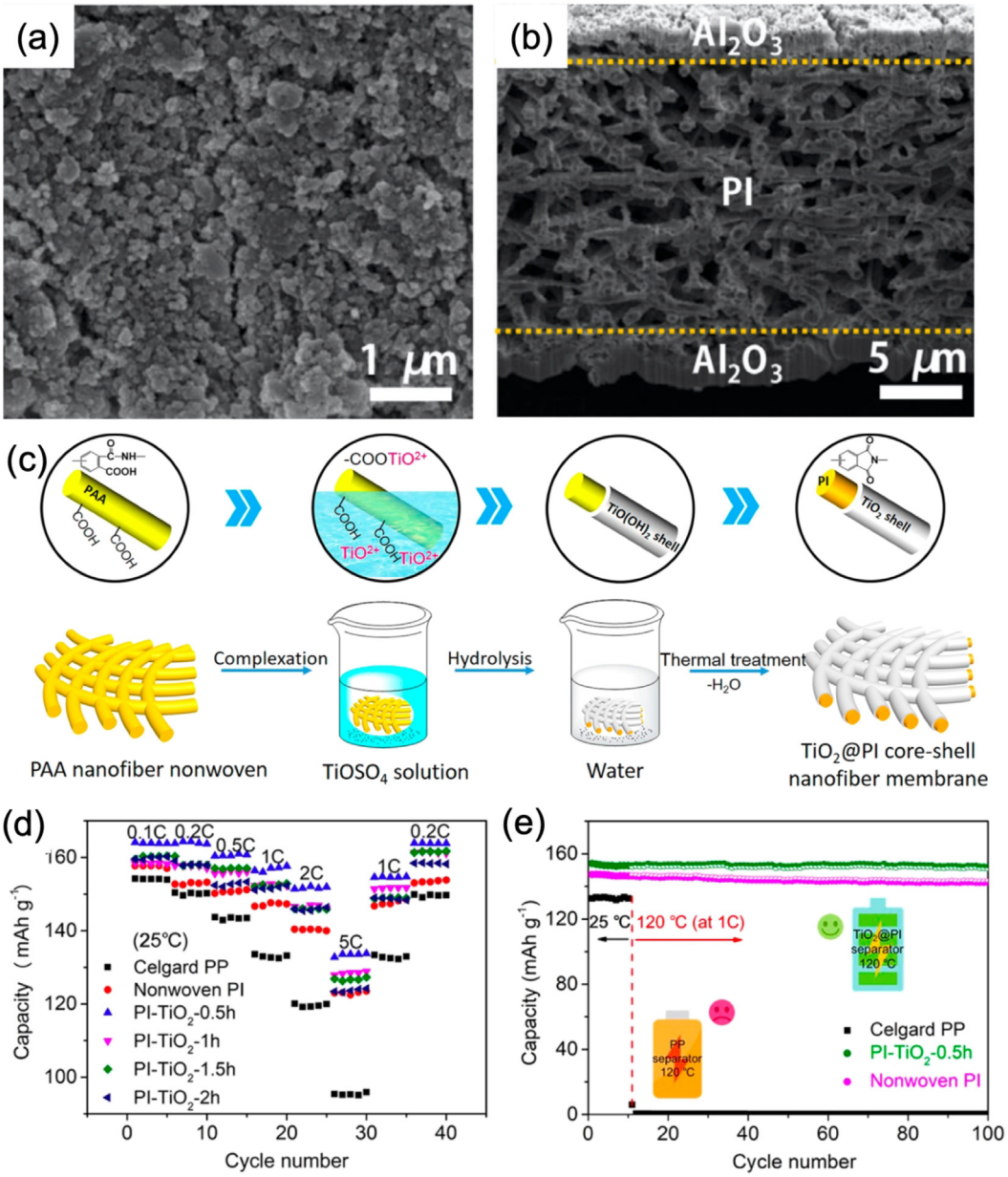

Fig. 10. (a) Surface and (b) cross-sectional SEM images of the Al_2O_3–PI separator. Reproduced with permission [94]. Copyright 2014, Elsevier Publications. (c) Schematic showing the fabrication of TiO_2@PI core–shell nanofiber membrane, (d) high rate capability at 25 °C, and (e) cyclic performance of the $LiFePO_4$||separator||Li half cells at 25 and 120 °C using Celgard® PP, PI nonwoven, and PI–TiO_2 hybrid separators. Reproduced with permission [87]. Copyright 2019, American Chemical Society.

by Dong and coworkers [87,95,96]. As shown in Fig. 10(c), TiO_2 nanolayer-coated PI nanofibers were fabricated by *in-situ* hydrolysis deposition [87]. The uniform TiO_2 coating not only improved the physical properties of the electrospun mats/membranes, including porosity, liquid electrolyte uptake, mechanical properties, and thermal dimensional stability but also provided superior ionic conductivity, thus resulting in good electrochemical stability and excellent rate capability. The $LiFePO_4$||Li battery using the PI–TiO_2 hybrid separator showed a much better rate capability, with an impressive capacity of 90 mAh g^{-1} at 5C, as shown in Fig. 10 (d). More importantly, the battery equipped with the PI–TiO_2 hybrid separator maintained excellent cyclic performance at 120 °C, whereas the one with the PP separator lasted for only 2 cycles because of the failure of the Celgard® PP (Fig. 10e). Boehmite (AlOOH), a flame retardant, has also been introduced as a coating material for PI separators [88]. Because AlOOH can be well dispersed in water, a water-based tape casting process was used to modify the PI fiber with AlOOH. Benefiting from the good thermostability of PI and the flame-retarding property of AlOOH, the composite separator showed excellent thermal stability and fire resistance (self-extinguishing).

As mentioned in Section 5.2.1, a sandwich-like PI/low-melting-point polymer/PI separator has a thermal shutdown function. To further improve the mechanical properties and thermal stability of the electrospun PI membrane, SiO_2 nanoparticles are incorporated. Liu et al. proposed a tri-layered SiO_2@PI/*m*-PE/SiO_2@PI nanofiber composite membrane for LIB separators [97]. The SiO_2@PI nanofibers were prepared using needleless electrospinning based on the fractal theorem. Ethylcellulose was then coated onto the PE and PI membranes to increase the affinity between the membranes. Finally, the PE membrane was sandwiched between two PI nanofiber membranes, followed by thermal calendering treat-

Table 2
A summary of characteristics of the PI-based separators used in LIBs.

Separator	Preparation method	Thickness (μm)	Tensile strength (MPa)	Electrolyte uptake (%)	Conductivity (mS cm^{-1})	Battery (cathode|| anode)	Electrochemical performance	Ref.
PI nanofiber nonwoven	electrospinning	40				$Li_4Ti_5O_{12}$||Li	~160 (0.2C)~100 (10C)	[57]
Hot-press PI nonwoven	electrospinning and hot pressing	23.3 ± 1.5	~22	61.2 ± 1.9		$LiNi_{0.5}Co_{0.2}Mn_{0.3}O_2$|| Graphite	110 (5C)	[59]
Crosslinked PI nanofiber mat	electrospinning	55	37.5	279	2.88	$LiFePO_4$||Li	130 (5C)	[60]
Fluorinated polyimide nanofibers	electrospinning	35	31.7	620.2	1.14	$LiFePO_4$||Li	89 (5C)	[62]
Co-PI nonwoven	blow spinning	24	12.95 ± 0.55	479.1	1.74	$LiCoO_2$|| Li	142.3 (0.2C)81.5 (5C)	[65]
Al_2O_3/PI-coated PP	dip-coating	25			0.95	$LiMn_2O_4$	98.6 (0.2C)	[70]
PI/PET-layered composite mats	electrospinning	40	50.87	220	0.897	$LiCoO_2$ ||Li_2TiO_3	125 (10C)	[71]
PE coated electrospun PI composite membrane	electrospinning and spin coating	30		1350%	1.2	$LiFePO_4$||MCMB	104 (1C)85 (2C)	[76]
PI-core@PBI-sheath nanofibers	electrospinning and dip-coating	12	59	208	1.7	$LiFePO_4$||Li	158.6 (0.1C) 130.9 (5C)	[77]
Side-by-side TPU/PI membrane	electrospinning	40 ± 2	8.87	665 ± 6	5.06	$LiMn_2O_4$||Li	~105 (1C)~70 (20C)	[78]
Multicore–shell PI-reinforced PVDF nanofibers	electrospinning	~20		427	1.3	$LiCoO_2$||MCMB	141 (1C)	[79]
Core–sheath PI@PVDF-HFP composite nanofibers	coaxial electrospinning	35	53	470	1.68	$LiCoO_2$ ||Li	116 (4C)100 (8C)	[82]
Sandwiched PI/PVDF/PI	electrospinning	50	8.2	476	3.46	$LiMnO_2$||Li	114.8 (0.5C) 108.9 (2C)	[84]
Tri-layer PBEI nanofiber mats	electrospinning	55	46.5	196.5	2.28	$LiFePO_4$||Li	160.2 (0.1C) 142.4 (5C)	[22]
GF/PI	dip-coating	46	10.4	210	0.38	$LiFePO_4$||Li	143 (0.2C)	[72]
PI-SiO_2 membrane	electrospinning	20	4.66	2400	2.27	$LiMn_2O_4$||Li	108 (0.2C)80 (5C)	[92]
Sandwiched Al_2O_3-coated PI	electrospinning and dip-coating	27		440.2	0.364	$Li(Ni_{0.5}Co_{0.2}Mn_{0.3})O_2$/$LiMn_2O_4$ ||graphite	~135 (0.2C)~100 (10C)	[94]
PI-TiO_2 core–shell nanofibers	electrospinning and *in-situ* hydrolysis deposition	27	27.6	460	1.54	$LiFePO_4$ ||Li	164 (0.2C)135 (5C)	[87]
AlOOH coated PI membrane	electrospinning and casting	28		337.5	2.18	$LiCoO_2$||Li	162 (0.5C)137 (4C)	[88]
Tri-layer SiO_2@PI/m-PE/SiO_2@PI composite membrane	electrospinning and thermal calendaring	32	177.6	575	0.941	$LiCoO_2$||Li	162.4 (0.2C)	[97]

ment for enhanced interfacial adhesion and mechanical strength. The resultant SiO_2@PI/*m*-PE/SiO_2@PI composite separator was expected to thermally shut down at temperatures above 131 °C and thermally run away at temperatures above 400 °C.

In summary, attributed to the improved wettability of the nanofiber mat and facilitated electrolyte absorption after the incorporation of hydrophilic ceramic particles, PI composite nanofiber separators containing inorganic nanoparticles (SiO_2, Al_2O_3, TiO_2, and AlOOH) have shown improved electrolyte uptake capability and ionic conductivity. In addition, the thermal stability and flame resistance of the PI/inorganic composite separators were improved. Table 2 compares the characteristics of the electrospun PI-based separators used in LIBs.

6. PI membranes for beyond lithium-ion chemistries

6.1. Lithium metal batteries

In commercial LIBs, the active materials on the anode side are either graphite or $Li_4Ti_5O_{12}$, both utilizing the intercalation mechanism to store Li^+. On some occasions, silicon or other types of alloying/conversion-type anode materials are mixed with graphite to achieve a higher specific capacity. Nevertheless, these chemistries based on either Li^+ intercalation or partial alloy/conversion struggle to satisfy the increasing demand for batteries with extreme energy densities. However, Li offers a much higher specific capacity (3860 mAh g^{-1}) at an extremely low electrode potential (-3.04 V vs. standard hydrogen electrode), making it an ideal anode material for Li-based batteries. More importantly, the Li metal anode may enable advanced cathode chemistries with high capacities but relatively low redox potentials such as Li–S and Li–O_2. Despite these advantages, Li metal anodes have been abandoned in the past few decades owing to safety issues induced by its high reactivity to electrolytes and the "dendrite" growth. When batteries with Li metal anodes are cycled, dendritic Li tends to grow and penetrate the separator, causing hazardous safety issues. Moreover, it constantly reacts with the liquid electrolyte during cycling, consuming Li^+ in the cells and forming a thick solid electrolyte interphase (SEI), which eventually shuts down the cells [98]. In fact, these are the reasons why LMBs were abandoned by Exxon in the 1970 s and by Moli Energy in 1989.

In the past decade, there has been a renewal of LMB research, and a number of methods have been proposed to mitigate the instability issues of Li metal anodes, including the design of novel electrode coatings and new electrolytes [99–101], changing the battery working conditions by applying external pressure or pulse charging [102,103], adopting predeposited films that can alloy with Li metal [104,105], and fabricating novel separators or SEs to mechanically block the dendrites [106–108]. There are many comprehensive reviews on these topics. In this paper, we only compile the advances in using PIs to stabilize Li metal anodes or to detect Li dendrites.

6.1.1. Bifunctional separators for dendrite detection

Despite many efforts over the decades, the dendrite growth problem in LMBs still cannot be fully resolved. Therefore, early detection of the penetration of Li dendrites is desired. In such situations, the batteries could be shut down in advance to prevent the anticipated short circuit and potential TR. Early detection could be accomplished by introducing an electron conductive layer between the two electrodes to measure the potential of the layer. When the dendrite reaches the layer, the electrode potential of the layer drops to 0 vs. Li/Li^+ owing to the short circuit. Based on this idea, Lin and coworkers developed an all-integrated bifunctional separator based on a microporous PI film. Such a separator has three layers, i.e., two porous PI layers with an electron conductive Cu layer in between [46]. As shown in Fig. 11(a)–(d), by measuring the electrode potential between the Li metal anode and the Cu layer, early detection of the dendrite is achieved, and the cells can be shut down before the dendrites reach the cathode to form a hard short. In their design, the PI porous layer was fabricated by a templating method, where LiBr was used as the sacrificial agent, which was washed away during post-processing. More

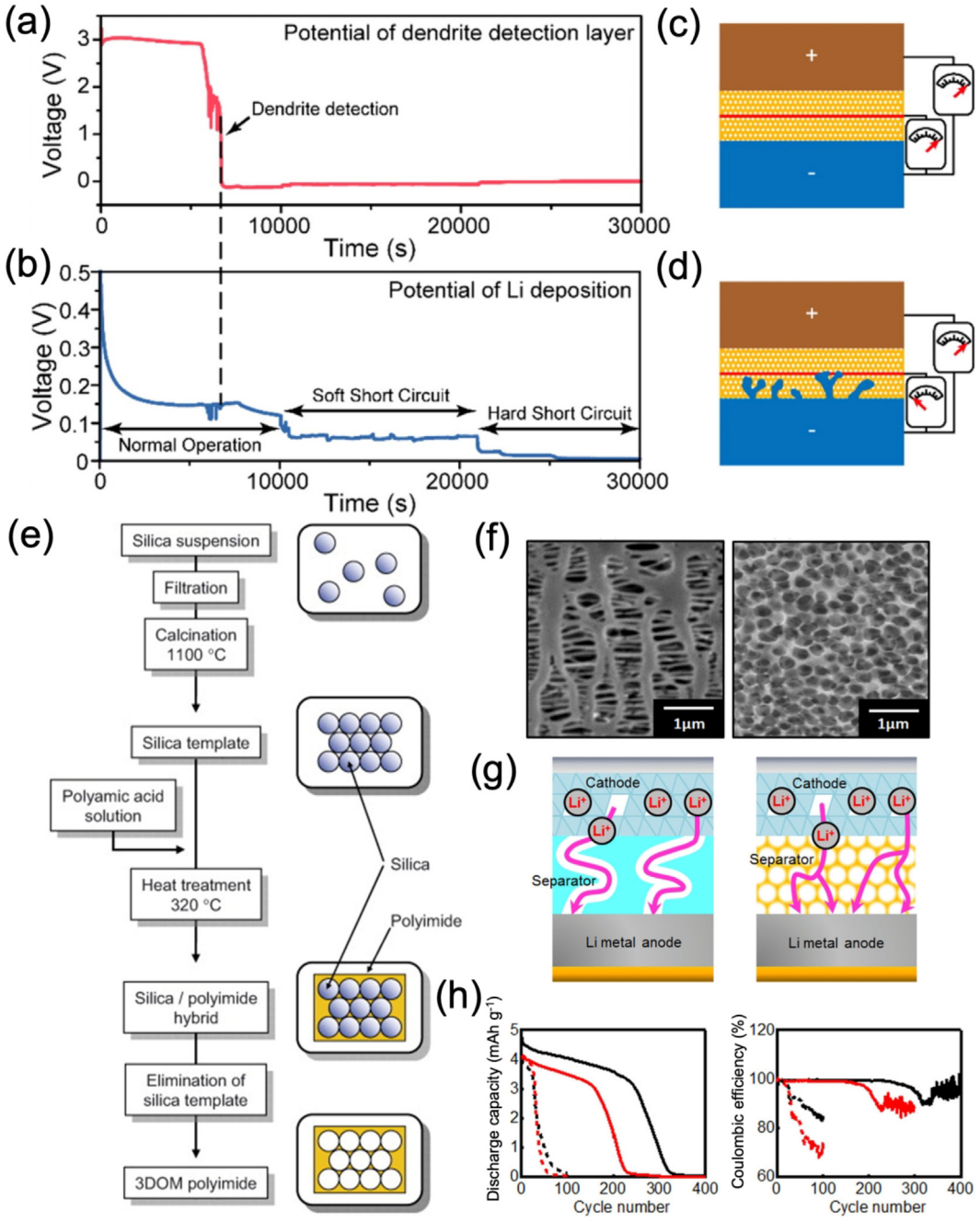

Fig. 11. (a) The voltage profile when monitoring the Cu layer versus Li^+/Li ($V_{Cu\text{-}Li}$) during Li deposition onto the negative electrode. (b) The voltage profile ($V_{Li\text{-}Li}$) of Li deposition from the positive electrode to the negative electrode. (c) and (d) Illustration of the dendrite growth and the electric response in the batteries with the bifunctional separator. Reproduced with permission [46]. Copyright 2016, American Chemical Society. (e) Schematic of the synthesis route of 3DOM PI separator. (f) Surface morphology of PE and 3DOM PI separators. (g) Illustration of the lithium transport pathways inside PE and 3DOM PI separators. (h) Cyclic stability of lithium metal batteries based on PE and 3DOM PI separators. The red curves and black curves represent data obtained from batteries with PE and 3DOM PI separators, respectively. The dotted line and the solid line represent $LiPF_6$/EC and $LiPF_6$/EC:EMC = 3:7 electrolytes, respectively. Reproduced with permission [43]. Copyright 2019, American Chemical Society.

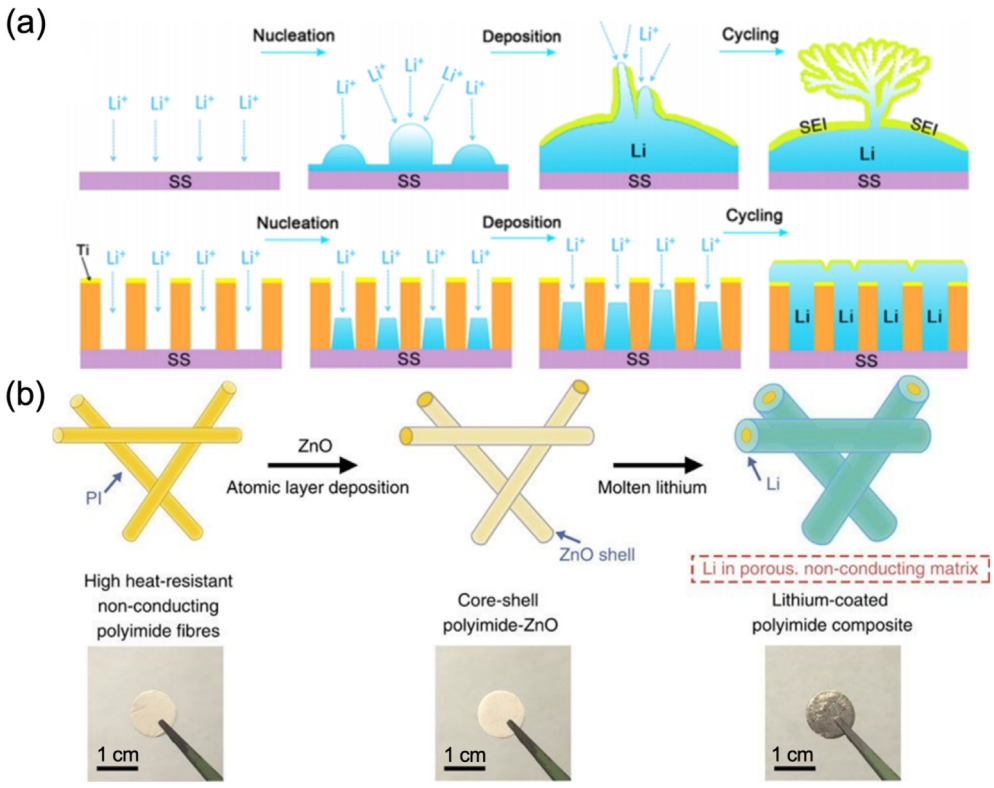

Fig. 12. (a) Illustration of Li nucleation behavior on stainless steel (SS) and in the PI matrix with nanosized channels. Reproduced with permission [113]. Copyright 2016, American Chemical Society. (b) Schematic showing the fabrication of the composite Li metal anode and the digital images of the corresponding products. Reproduced with permission [114]. Copyright 2016, Springer Nature.

importantly, the good thermal stability of PI films enables them to be processed at high temperatures, and a thin Cu layer can be deposited using sputtering.

6.1.2. PI-based separators as dendrite mitigators

In addition to the dendrite-detecting feature introduced above, PI-based separators have also been developed to directly suppress the dendrite growth problem and mitigate the safety issue of LMBs.

The Kanamura group developed 3DOM PI separators using a colloidal crystal templating method [43,44,109–112]. Fig. 11(e) shows the fabrication process of such a separator [43]. In their procedure, silica particles with submicron diameters were dispersed in dimethylacetamide together with PAA. Then, the dispersion was cast onto the surface of a glass plate followed by drying at 60 °C. Next, the PAA precursor was converted to PI by thermal imidization at 320 °C, and the final separator was obtained by removing the silica particles in 10 wt% HF solution for 5 h. The resulting product was characterized as a 3D-ordered structure, which is significantly different from the one-dimensional pore structure of commercial polyolefin separators, as shown in Fig. 11(f). The 3DOM structure promotes the transfer of Li^+ in three dimensions and provides uniformly deposited Li owing to the uniform distribution of the current density, as illustrated in Fig. 11(g). Additionally, the 3DOM PI membrane has better wettability toward the electrolyte and can uptake a high content of liquids owing to its high porosity of ~ 70%. In fact, the 3DOM PI separator can host ethylene carbonate (EC) alone, a desired electrolyte solvent with a high dielectric constant and salt solubility, without mixing it with any linear carbonate esters such as ethyl methyl carbonate or dimethyl carbonate (DMC) to improve the wettability. In sharp contrast, EC can hardly permeate commercial PP separators. Because of its ability to regulate the current and its wettability by the electrolyte, the 3DOM PI separator exhibits considerably better performance in LMBs than commercial PP separators. As shown in Fig. 11(h), LMBs with 3DOM PI separators significantly outperformed those with commercial PP separators by displaying higher capacity and lasting longer in different ester-type electrolytes.

Despite the better performance of 3DOM PI separators, ester-type electrolytes are prone to side reactions with Li metal, leading to relatively low cycle numbers. Recently, a new concept of solvent-in-salt or concentrated electrolytes has been proposed. [43] Such electrolytes contain a high concentration of Li salts which change the solvation structure of the electrolyte, significantly improving the electrochemical stability toward the Li metal. However, the concentrated electrolytes usually wet poorly in the PP separators. Yuta et al. utilized a 3DOM PI separator to host a highly concentrated sulfolane-based electrolyte, which was easily wetted by the concentrated solution [43]. The resulting LMBs exhibited an outstanding average Coulombic efficiency of ~ 98% over 400 cycles at 1.0 mA cm^{-2} on the anode side. Full cells based on $LiFePO_4$ cathodes can be cycled for over 150 times without notable capacity decay.

To briefly summarize, the pore sizes, distribution of the pores, and molecular structures of the PIs have a significant influence on the Li deposition behavior, without any doubt. When designed properly, PI-based separators are very promising for stabilizing LMBs.

6.1.3. 3D PI-based frameworks as Li host

Apart from being used to fabricate separators, PIs are also excellent materials to make host frameworks for Li metal anodes because of their high chemical resistivity and good flexibility. The Cui group designed PI hosts with vertically aligned porous structures attached to stainless steel current collectors [113]. They

found that in nanosized channels with large aspect ratio, relatively equal Li^+ flux in each channel could be achieved, leading to homogeneous Li nuclei distribution and growth, as illustrated in Fig. 12(a). Therefore, the resulting Li metal anode is stabilized. By contrast, microsized confinement is much less effective in mitigating dendrite growth. This work by Cui et al. represents the early stage of utilizing PI as the host for Li metal anodes. However, the overall electron conductivity of PI is negligible, limiting the Li nucleation avenues and thus prohibiting the cycling of the LMBs at high current densities. The same group subsequently demonstrated another polymer matrix by electrospinning a nanofibrous PI skeleton and coating it with lithiophilic ZnO using atomic layer deposition, as shown in Fig. 12(b) [114]. Further infusion of Li into such a matrix results in the final composite Li metal anode, which displays outstanding stability in liquid electrolytes. In their design, PI was chosen because of its high stability against the highly reactive molten Li and its flexibility to accommodate the large volumetric changes during cycling. The ZnO layer was deposited to improve the wettability of molten Li toward the PI and to enable its infusion. The porous electrode can reduce the effective current density and flatten the voltage profiles. Stable cycling of more than 100 cycles was achieved at high current densities of up to 5 mA cm^{-2} in both carbonate and ether electrolytes.

More complex designs were reported after the initial study that displayed even better performance. Zou and coworkers fabricated microcompartmented anode arrays using PI and copper to confine the dendritic growth of Li in the lateral direction [115]. In their design, 3D PI-clad copper current collectors were fabricated using laser ablation. Owing to the geometric features, the dendrites were retained inside the compartmented copper current collector. This electrode exhibited superior cycling stability, with over 150 cycles of smooth running at 0.5 mA cm^{-2}. Their design inspired the further development of PI-based complex hosts for lithium metals. Recently, our group designed a laser-induced graphene hierarchical structure on copper foil (LIGHS@Cu) based on laser processing PI [116]. By scribing PI films onto Cu foils with a laser, a 3D hierarchical composite material was constructed, which consisted of a highly conductive Cu substrate, a pillared array of flexible PI, and porous LIG on the walls of the PI pillars. Such composites enabled ultrastable Li metal anodes with Coulombic efficiencies > 99% and full $LiFePO_4$-based cells stably operated under practical conditions, i.e., a limited N/P ratio of 5 and high active material loading of ~ 15 mg cm^{-2} over 250 cycles. This extraordinary performance originates from the abundant defects in LIGs, which facilitate the Li nucleation kinetics, the 3D hierarchical structure that directs the lateral growth of Li, and the flexibility of the PI framework, which accommodates the large volumetric change of Li during cycling.

6.2. Lithium–sulfur batteries

In conventional LIBs, the cathodes are transition metal oxides that utilize intercalation-type chemistries to store Li ions. Although facile Li^+ hopping in predefined diffusion channels endows these materials with good cyclic reversibility and fast kinetics, the limited number of active sites in the structures practically restricts the specific capacity, which typically remains under 200 mAh g^{-1}. However, conversion/alloy-type cathodes have drawn considerable attention owing to their extremely high specific capacity. Among the advanced cathodes, elemental S is one of the most promising materials because it displays an extremely high theoretical capacity of 1675 mAh g^{-1} via the reaction shown below [117]:

$$\text{Charge: } S_8 + 16Li^+ + 16e^- \rightarrow 8Li_2S$$

$$\text{Discharge: } Li_2S \rightarrow 1/8S_8 + 2Li^+ + 2e^-$$

Therefore, LSBs can deliver energy densities higher than 600 Wh kg^{-1} in lab-scale pouch cells, which can potentially be increased to over 800 Wh kg^{-1} upon further development. Despite the extremely high energy densities, LSBs suffer from a number of critical issues. First, the kinetics of the electrode reactions are slow because neither Li_2S nor S are good conductors for electrons and Li ions. Such poor kinetics have constituted the major bottleneck for early-stage development of room-temperature LSBs. Over the past two decades, it has been discovered that by substituting ester carbonates into ether-type solvents, LSBs could be reversibly cycled, and the batteries display a high discharge capacity close to their theoretical limit [118–120]. This was later found to originate from the facilitated kinetics owing to the solubility of the intermediate discharge products such as Li_2S_4 and Li_2S_6, as shown in Fig. 13(a) [117]. Although these soluble polysulfides enable fast conversion between Li_2S and S, they diffuse between the cathode and anode, leading to the so-called "shuttling effect." As illustrated in Fig. 13(b), during battery operation, the polysulfides are reduced to insoluble Li_2S and polysulfides with a shorter chain length on the anode side. These reduced sulfides recombine with other polysulfides in the electrolyte, which subsequently diffuse back to the positive electrode and get oxidized again [121]. Significant self-discharge and fast capacity degradation occur. Extensive effort has been devoted to mitigating the "shuttling effect." One of the most promising methods is to trap the polysulfides using highly polar materials to restrain their diffusion to the cathode side. Although doped carbon and transition metal oxides have been the mainstream absorbers, PIs have also been found to strongly adsorb the polysulfides, which can be illustrated using a simple absorption experiment [122]. Combined with good mechanical strength, low density, and good chemical resistivity, many PI-based strategies have been explored and show good promise to mitigate the shuttling issue.

6.2.1. PI-based separators for polysulfide capture

Owing to the abundant nitrogen and oxygen in the acylamino groups of PI, PI separators have a strong ability to capture polysulfides through electrostatic interactions, prohibiting the shuttling of soluble polysulfides [122]. In addition, the strong effect on adsorbing polysulfides can prevent the side reaction between Li and polysulfides, restraining the corrosion of Li and Li dendritic growth. Finally, the excellent heat-resistant properties of PI separators can also improve the safety of batteries. Therefore, PI-based separators have been studied in LSBs for polysulfide capture. Miao et al. reported the fabrication of PAA nanofiber separators with dual functions for LSBs via a facile electrospinning process [123]. The –COOH groups simultaneously facilitated the diffusion rate of positively charged Li^+ and inhibited the "shuttle effect" of the negatively charged polysulfide anions via Coulombic interactions. Consequently, the PAA separators displayed outstanding electrolyte wettability and uptake and superior battery performance, with a high capacity retention of 781.8 mAh g^{-1} (76%) after 200 cycles at 0.2C. Wang and coworkers first proposed the use of an electrospun PI separator to confine the polysulfide [122]. By soaking the PI separators in a polysulfide solution and then washing them, they found that the separator was able to reversibly adsorb and desorb polysulfides, as shown in Fig. 13(c). They further assembled LSBs using the PI separator and found that the cyclic stability and discharge capacity were significantly better than those using conventional PP separators, despite the electrolyte used. The better polysulfide adsorption ability comes from the strong electrostatic interaction between polysulfides and the lone-pair electrons donated by the nitrogen and oxygen of the acylamino groups of PI. The Cheng group verified their results by utilizing a hot-pressed electrospun PI separator [124]. Apart from pure PI, other materials have been mixed with PI to achieve even

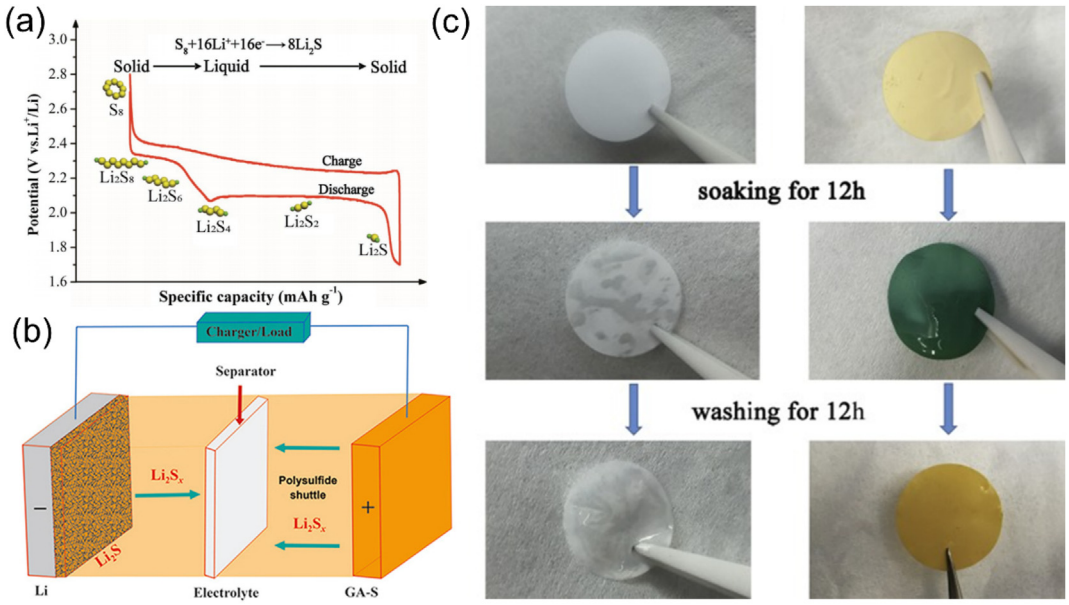

Fig. 13. (a) The chemically active species during charge and discharge of LSBs in typical ether-type electrolytes. Reproduced with permission [117]. Copyright 2017, Wiley-VCH Publications. (b) Illustration of the polysulfide shuttling effect. Reproduced with permission [121]. Copyright 2017, Elsevier Publications. (c) Digital images of PE and PI separators after soaking in polysulfide-containing solvents and after subsequent washing using solvents without polysulfides. Reproduced with permission [122]. Copyright 2017, Elsevier Publications.

better performance [125–129]. Wang et al. prepared a composite separator by loading graphdiyne onto PI [130]. Graphdiyne has a strong affinity for polysulfides because of the strong chemical bonds formed. Ascribed to the combination of two good adsorbers in the separator, the final battery exhibited excellent stability after 200 cycles, with 816.7 mAh g^{-1} being retained. Zhou et al. took this a step further and fabricated a composite separator consisting of more components [131]. In their design, a sandwich structure composed of carbon nanoparticles coating the S-composite cathode and a PEO-integrated $Li_7La_3Zr_2O_{12}$coating toward the Li metal was prepared. With such a complex design, a high specific capacity of 1474.3 mAh g^{-1} without severe overcharge behavior was demonstrated at a high temperature of 100 °C. The LSBs using such a separator delivered excellent cycling stability, with only 0.2% capacity decay per cycle over 200 cycles at 80 °C at a high rate of 5C.

6.2.2. PI-based redox mediator in cathodes

Apart from being used as separators, PIs have also been used in cathodes. It is known that PIs are electrochemically active within the potential range of 1–3 V vs. Li/Li^+ due to the carbonyl group in their structures [132–135]. Because the electrochemically active voltage window overlaps with that of sulfur, PIs can be used as redox mediators for LSBs, i.e., as reversible redox couples that facilitate the electrochemical reaction of the electrode with reduced polarization and enhanced active material utilization. In 2016, the Zhang group proposed the idea of incorporating PI particles into the cathode of LSBs [136]. Specifically, they prepared various types of PI compounds as hosting matrices whose molecular structures are shown in Fig. 14. These PI–S composites exhibited higher S utilization and better cycling stability than pure sulfur, with a discharge capacity of 574 mAh g^{-1} at the 450th cycle. Hernández and coworkers later carried out a more detailed study and proposed the concept of PI-based redox mediators for LSBs [137]. In their design, three PI–polyethers were synthesized and incorporated into the sulfur cathode. Because of the overlap of the redox potential range, the PIs served as redox mediators for S reduction and oxidation, whereas the polyether trapped the polysulfides, as illustrated in Fig. 14. By incorporating these redox-active polymers, the carbon content can be greatly minimized in the composite cathode while maintaining good reversibility and reaction kinetics. In their best results, even when the amount of carbon black in the cathode was reduced to 5 wt% (compared with the > 30 wt% in normal cases), the cells still delivered 500 mAh g^{-1} at 0.2C, with 78% capacity retention after 20 cycles.

6.2.3. PI-based redox mediator in cathodes

Owing to the high carbon content and ease of morphology control, PIs are widely used as carbon sources to synthesize carbon-based nanomaterials. Owing to their high electron conductivity, large surface area, and good affinity for polysulfides, these materials are also good hosts for S in the cathodes. Wang et al. fabricated an activated carbon nanofiber interlayer by thermally treating an electrospun PI mat [138]. By inserting such a layer between the separator and the cathode, the cyclic stability of an LSB was significantly improved. The battery showed no capacity decay after 100 cycles. Tejassvi et al. confirmed the effectiveness of such a strategy and found that the excellent polysulfide capturing ability of a carbon nanofiber interlayer comes from both the high surface area and a large number of dopants [139].

6.3. Solid-state batteries

In conventional LIBs, electrolytes are made of organic ester/ether solvents and various types of dissolved salts. These compounds are extremely volatile and flammable. TR and even explosions in extreme cases occur when the batteries are not managed properly or are damaged, causing severe safety hazards. In addition to safety concerns, liquid electrolytes are prone to side reactions when Li metal is used as the anode, as mentioned in Section 6.1. Therefore, they practically limit the energy density of current LIBs. In principle, by replacing conventional liquid electrolytes with a Li-conducting solid, both the safety and the electrochemical stability issues can be resolved. Therefore, such devices, i.e., solid-state batteries (SSBs), are considered the ultimate form of LIB, offering not only extreme safety but also high energy density [140,141]. In

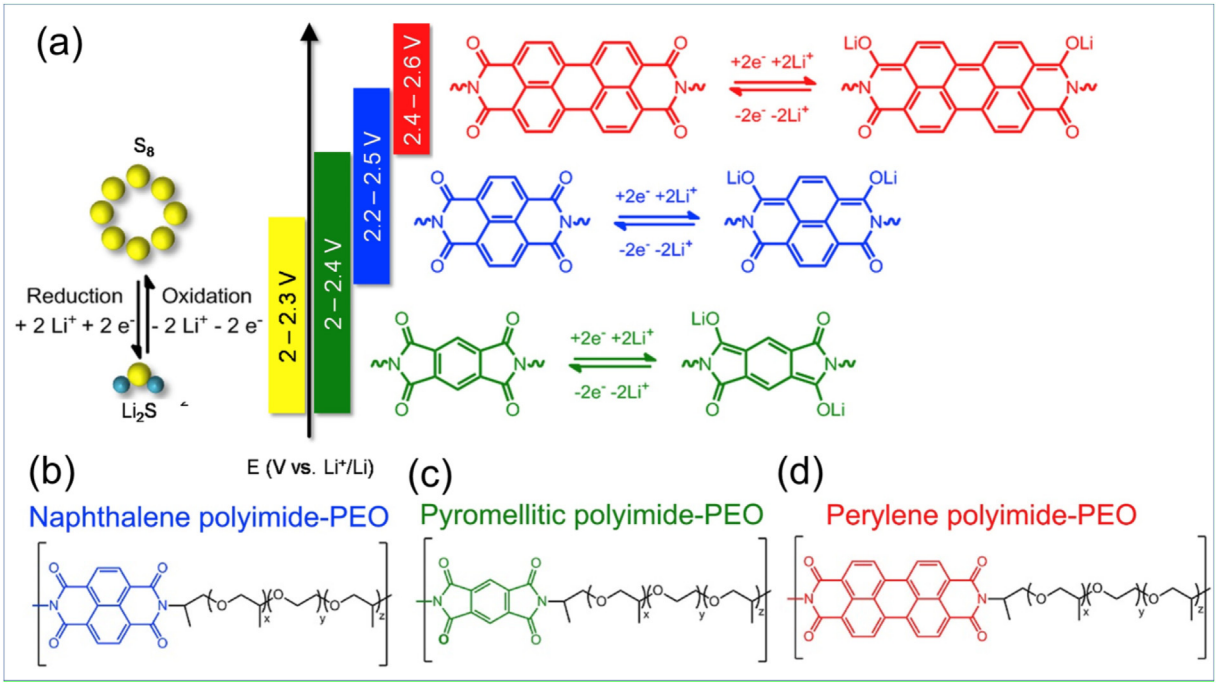

Fig. 14. Schematic of (a) the redox potentials of S and PI monomers, (b) the molecular structure of naphthalene PI-PEO, (c) pyromellitic PI-PEO, and (d) perylene PI-PEO. Reproduced with permission [137]. Copyright 2017, Elsevier Publications.

SSBs, SEs not only serve as the separator to physically block contact between the cathode and the anode but also as the main Li^+ transport media. Therefore, as an essential part of SSBs, there are a number of requirements for the properties of SEs: They need to 1) be Li-ion–conductive, 2) be electronically insulating to prevent internal short circuit and self-discharge, 3) have a wide electrochemical window to prevent degradation, and 4) be mechanically strong to suppress the growth of lithium dendrites.

Although pristine PI films fulfill most of these requirements, the lack of flexible side chains and Li coordination sites in their molecular structure makes them non-Li-conductive and unsuitable for use as SEs directly. Therefore, Li-conductive components should be incorporated either on the molecular level or on the microscale to enable the Li ions to pass through. Two types of SEs made from PIs have been fabricated based on these two strategies: PI-based single-phase electrolytes, where Li-conductive side chains are included at the molecular level, and PI-based composite SEs, where PIs are mixed with other Li-conducting SEs to form composites.

6.3.1. PI-based single-phase electrolytes

Because of the lack of efficient Li transport mechanisms in intrinsic PIs, modifications of PIs to incorporate Li-conductive branches or units are necessary to fabricate SEs with acceptable ionic conductivities. Among the polymers that can transport Li^+, PEO has attracted the most attention because ethylene oxide (EO) units have a high donor number and can coordinate Li^+ in a similar way that organic carbonates do. Together with the high chain flexibility, the Li ions can effectively transport in PEO, as shown in Fig. 15(a) [142]. Therefore, copolymerization with PEO or the incorporation of branches with ether groups is deemed one of the most promising methods to fabricate PI-based solid polymer electrolytes.

In 2003, Meador and coworkers designed a series of "rod–coil" block copolymers with PI and polyether segments and studied their performance as solid polymer electrolytes for SSBs [143]. The copolymers consisted of short, rigid PI segments and flexible PEO coil segments, as shown in Fig. 15(b). The flexible coil phase (Jeffamine XTJ-502) with ether groups allows the conduction of Li^+, whereas the rigid PI blocks phase-separate from their coil counterparts to form nanodomains. Interestingly, phase separation leads to abundant interfaces that influence the solid behavior and Li^+ transport, especially at low temperatures. In fact, the highest conductivity of polymers in this family was 3×10^{-5} S cm^{-1} at room temperature. At 0 °C, its ionic conductivity was comparable to that of the room-temperature PEO films, as depicted in Fig. 15(c). Despite the relatively good ionic conductivity, the electrochemical window and the full cell performance have not been reported. Xue et al. subsequently followed up on PI-PEO rod–coil block copolymers and studied the detailed physical properties of polymers with T-shaped PI rods [144]. They carried out differential scanning calorimetry (DSC) and atomic force microscopy (AFM) analyses on these polymers and confirmed the formation of nanodomains during the phase separation of PI and PEO. Based on their results, they proposed a microphase separation model to describe the structure of the copolymer. As shown in Fig. 15(d), the phase separation between the PEO crystals and imide rods directs the main chains to form a lamella-like structure.

Apart from the copolymerization from existing segments, grafting Li-conductive side chains to the backbone of the polymer is another strategy that enables the fabrication of PI-based solid polymer electrolytes. In 2010, Higa and coworkers synthesized a graft copolymer consisting of a PI main chain and a PEO-based side chain; its structure is shown in Fig. 16(a) [145]. The preparation involves the synthesis of a macro-initiator, i.e., chloromethylated PI. This process was carried out by the reaction of 4,4-(hexafluoroisopropylidene) diphtalic anhydride/4,4-diaminodiphenyl ether polyimide (6FOD), followed by chloromethylation of the obtained PI with chloromethyl methyl ether to introduce a chloromethyl group into the PI main chain. Then, poly[(oxyethylene)$_x$ methacrylate] (POEM) side chains were grafted onto the macro-initiators using atom transfer radical polymerization to synthesize a 6FOD-*g*-$POEM_9$ grafted copolymer. Finally, the solid polymer electrolyte was prepared by adding $LiClO_4$ salt. The ionic conductivity of the resulting electrolyte

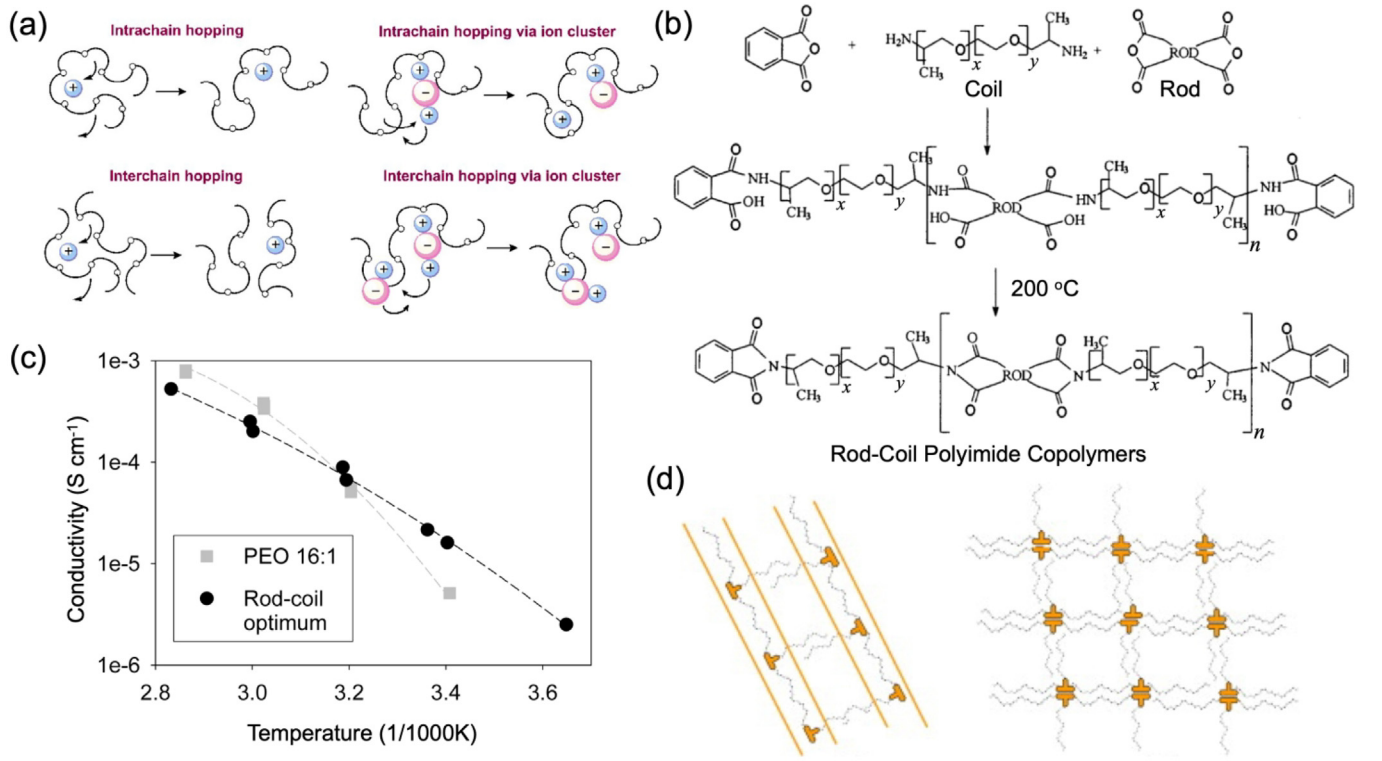

Fig. 15. (a) Illustration of the mechanism of ion transport in PEO. Reproduced with permission [142]. Copyright 2015, Royal Society of Chemistry. (b) The synthesis route of the rod–coil PI copolymers. (c) Ionic conductivity of the rod–coil PI copolymer. Reproduced with permission [143]. Copyright 2003, American Chemical Society. (d) Illustration of the structures of the rod–coil PI copolymer. Reproduced with permission [144]. Copyright 2006, Elsevier Publications.

increased with increasing side chain length, and the highest value was 6.5 × 10^{-6} S cm^{-1} at 25 °C when the POEM content was 60 wt%.

Apart from the abovementioned solid polymer electrolytes based on aromatic PIs, other types of PIs have also been explored. Öztürk et al. prepared a naphthalene-based PI electrolyte and studied its ionic conductivity and electrochemical window [146]. The synthesis route and final structure of PI are shown in Fig. 16(b). Unfortunately, these PIs alone are not ion-conductive, and PEO needs to be incorporated before the thermal imidization of the PAA. Therefore, there is no direct chemical bonding between the PI and PEO, and the final product is either a polymer solution or a blend. The conductivity of the electrolyte was 3.7 × 10^{-5} S cm^{-1} at RT when a large amount of PEO was incorporated.

6.3.2. PI-based composite solid electrolyte

Although PIs are not intrinsically conductive enough to serve as SEs for SSBs, their high mechanical strength and good thermal resistance make them ideal supporting structures for other SEs. More importantly, the interfaces between PIs and the ionic conductive phase may provide additional avenues for fast ion conduction, thereby facilitating ion transport. Therefore, mixing PI frameworks with other ion-conductive materials to form composite solid electrolytes (CSEs) is another promising strategy to fabricate PI-based SEs. These ionic conductive SE fillers can be organic polymers such as PEO, solidified small molecules such as succinonitrile, or inorganic materials such as argyrodite-type phosphosulfides [147,148].

PEO is a promising SE, but it suffers from low ionic conductivity and relatively low mechanical strength, especially at high temperature and when it is doped with a large amount of Li salts. Also, the thickness of PEO is not easy to control using conventional casting and drying methods, resulting in high areal-specific resistance. Wan and coworkers fabricated an ultrathin solid polymer composite electrolyte (PI/PEO/LiTFSI) using PI hosts with vertically aligned channels to address these issues (Fig. 17a) [52]. They used a track-etching technique to create vertically aligned channels in commercial Kapton® PI films with a thickness of ~ 8 μm and infiltrated them with a PEO-based SE. The resulting composite SE was as thin as ~ 10 μm while still having relatively good mechanical strength stability (Fig. 17b). More importantly, it was characterized by fast Li^+ conduction, with conductivities as high as 2.3 × 10^{-4} S cm^{-1} at 30 °C because the abundant interfaces between the PEO and PI facilitated Li^+ transport along the aligned channels. Owing to the minimized thickness of the electrolyte, the energy density of the SSB increased dramatically compared with the conventional tape-cast PEO membranes, as shown in Fig. 17(c).

In 2020, Cui and coworkers followed up on this work and incorporated an additional fire retardant to further decrease the flammability of such an electrolyte [149]. As shown in Fig. 17(d) and (e), they fabricated an SE composed of a porous PI mechanical enforcer, a fire-retardant additive, decabromodiphenyl ethane (DBDPE), and an ion-conductive polymer electrolyte (PEO/LiTFSI). When heated, DBDPE degraded and generated Br• to capture the highly reactive radicals H• and OH• emitted by the burning electrolyte, terminating the combustion chain branching reactions. The self-extinguishing time of such an electrolyte significantly decreased from ~120 s g^{-1} of the intrinsic PEO/LiTFSI electrolyte to almost zero.

Even though these electrolytes display relatively good mechanical strength and good fireproof characteristics, their ionic conductivity is still relatively low because of the slow Li^+ transport in the polymer electrolyte. Therefore, it is difficult to cycle these batteries at room temperature. To solve this issue, Liu et al. incorporated succinonitriles as plasticizers into a polymerized ionic liquid [150]. The plasticizing effect changed the Li^+ transport mode, and the resulting electrolyte had a high ionic conductivity of 6.54 × 10^4 S cm^{-1}. An SSB based on a lithium metal anode and a $LiFePO_4$ cathode can be cycled at RT and still achieve a relatively

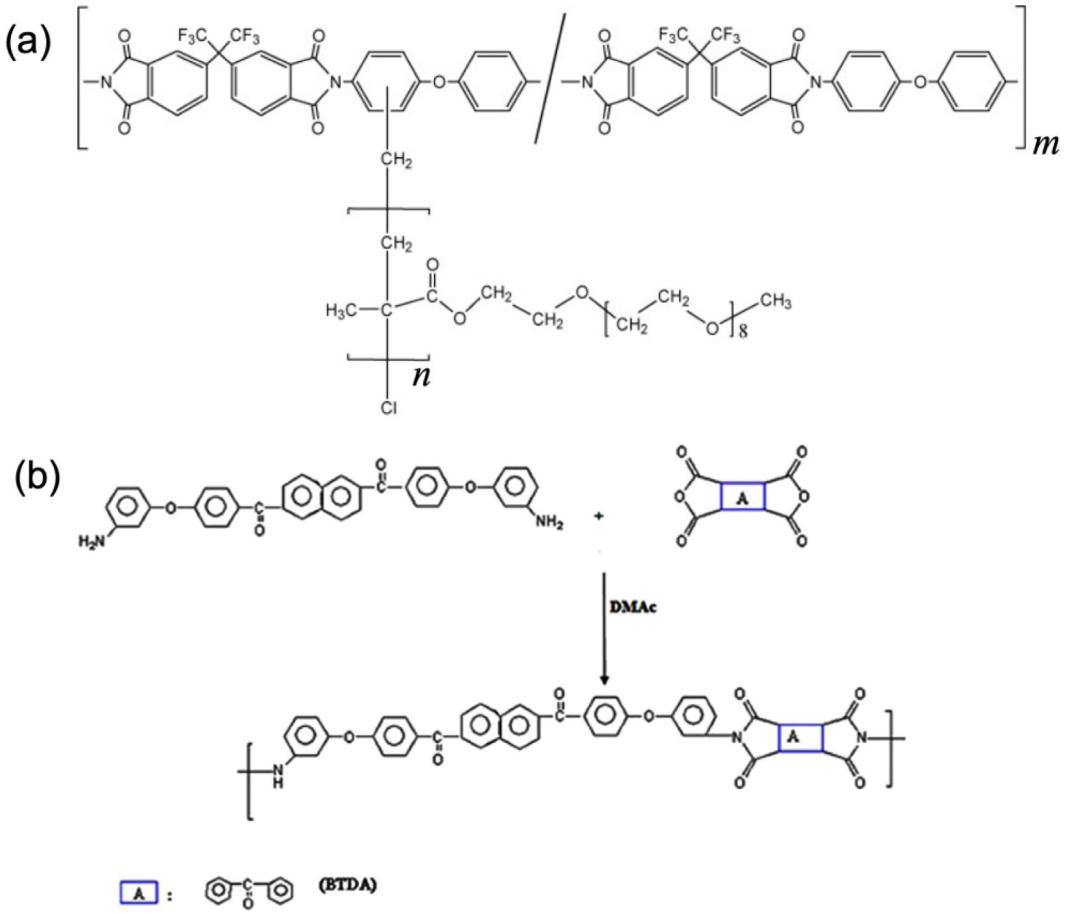

Fig. 16. Molecular structures and synthesis routes of (a) the PEO-grafted PI copolymer [145] and (b) the naphthalene-based PI electrolyte [146]. The two figures are reproduced with permission. Copyright 2010, Elsevier Publications; Copyright 2016, Wiley-VCH Publications.

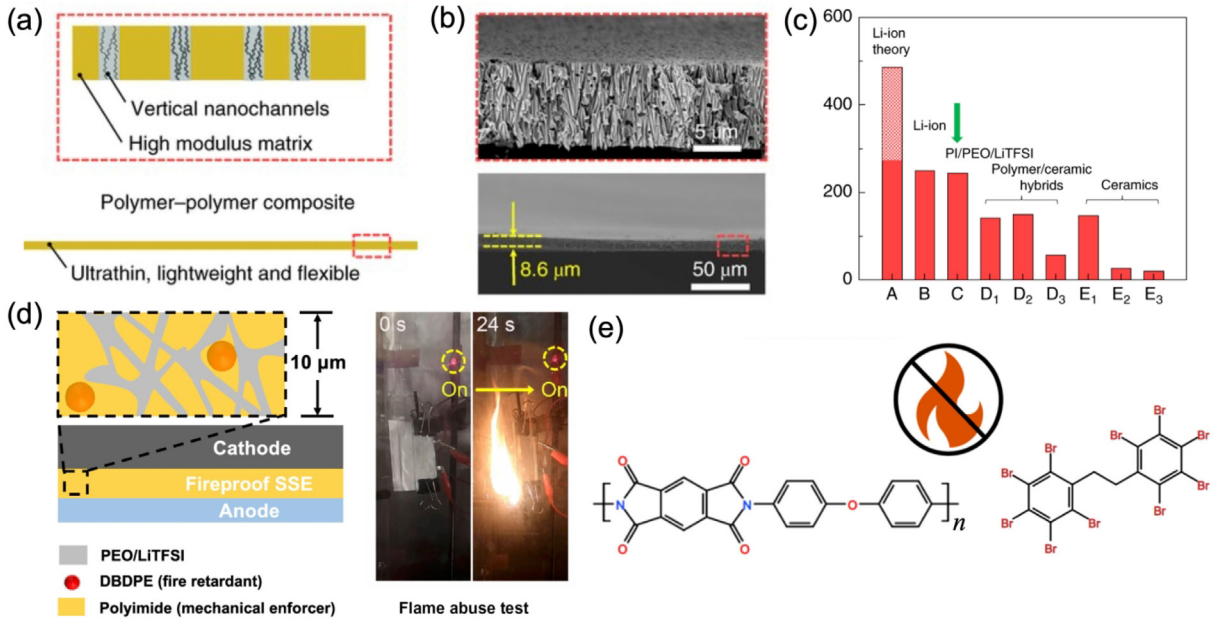

Fig. 17. (a) Schematic showing the design principles of (PI/PEO/LiTFSI) composite SSE. (b) Cross-sectional SEM images of an ultrathin nanoporous PI film (bottom) with a higher magnification image of the aligned nanopores (top). (c) Energy density chart of batteries where different electrolytes, battery casings, separators, and liquid/SEs are all taken into account. A and B denote LIBs based on PP separators. C denotes the SSB with the PI/PEO/LiTFSI SE. D_1–D_3 denote the batteries based on polymer/ceramic composite SSEs, where D_1 and D_2 refer to the $Li_7La_3Zr_2O_{12}$ (LLZO)/PEO/LiTFSI composites and D_3 is the SiO_2/PEO/$LiClO_4$ composite; E_1–E_3 denote the batteries based on ceramic-type SSEs, where E_1 is ultrathin LLZO, E_2 is regular $Li_{10}GeP_2S_{12}$(LGPS)-type SE, and E_3 is ceramic LLZO. Reproduced with permission [52]. Copyright 2019, Springer Nature. (d) Design principles of the fireproof and lightweight polymer–polymer solid-state electrolyte. (e) Molecular structures of the PI and DBDPE. Reproduced with permission [149]. Copyright 2020, American Chemical Society.

high capacity of 120 mAh g^{-1} at 0.5C. It is worth noting that, owing to the incorporation of plasticizers, such an electrolyte is not fully solid-state but rather quasi-solid or hybrid, sharing some resemblance to gel-polymer electrolytes.

To date, polymer-type SEs still suffer from low ionic conductivity, which usually does not surpass 10^{-3} S cm^{-1} at room temperature if no plasticizers are included. In sharp contrast, many inorganic SEs display significantly higher ionic conductivities of over 10^{-3} S cm^{-1}, and some even outperformed conventional liquid electrolytes, which are characterized by extremely fast ion conduction of > 10^{-2} S cm^{-1}. Among them, sulfide-type SEs are promising candidates for composites with the PI matrix because they can be synthesized via a solution-based route and thus can be easily incorporated into the PI matrix. Kim and coworkers reported the incorporation of a solution-processable $Li_6PS_5Cl_{0.5}Br_{0.5}$ solid electrolyte (which displayed a high ionic conductivity of 2 mS cm^{-1} at RT) into the PI matrix to form thin and flexible SEs [151]. They first prepared a PI scaffold using the electrospinning method, as shown in Fig. 18 (a)–(c). A detailed introduction of the electrospinning method can be found in Section 4.2.1. They then infiltrated the matrix with a homogeneous $Li_6PS_5Cl_{0.5}Br_{0.5}$/ethanol solution, followed by evaporation of the solvents and subsequent thermal treatment at > 180 °C to enhance the crystallinity of $Li_6PS_5Cl_{0.5}Br_{0.5}$. The resulting electrolyte was 40 μm thick and displayed good flexibility, as shown in Fig. 18(d). Owing to the thinness of the membrane, the final $LiNi_{0.6}Co_{0.2}Mn_{0.2}O_2$ (NCM)||graphite battery showed a relatively high areal capacity, as shown in Fig. 18 (e and f).

These are the two main types of SEs that can be incorporated into the PI matrix. A mixture of polymers and ceramics can also be combined with PIs. This family of mixed-type solid conductors is also known as composite SEs or CPEs. Hu et al. demonstrated this idea by incorporating a PVDF/$Li_{6.75}La_3Zr_{1.75}Ta_{0.25}O_{12}$ composite

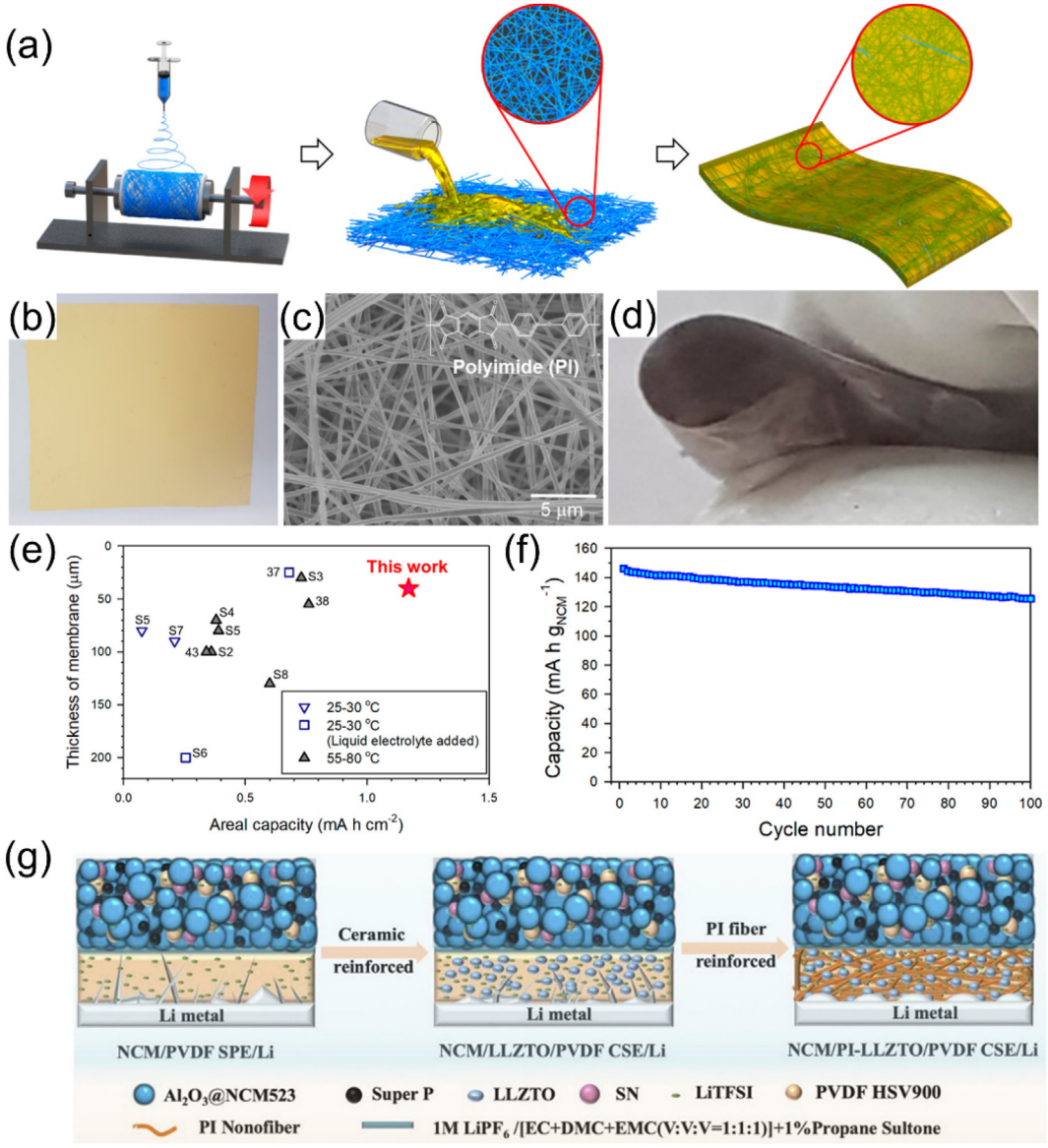

Fig. 18. (a) Schematic illustration of the fabrication of sulfide SE membranes for all solid-state batteries by infiltration of electrospun porous PI nanowires (NWs) with solution-processable Li_6PS_5[Cl, Br]. (b) Photograph and (c) SEM image of an electrospun porous PI NW. The sheet in (b) is 10 cm × 10 cm. (d) Photographs of a PI-$Li_6PS_5Cl_{0.5}Br_{0.5}$ membrane. (e) Comparison of SE membrane thickness and areal capacity for NCM||graphite all-solid-state full cells employing PI–$Li_6PS_5Cl_{0.5}Br_{0.5}$ membranes with other results. (f) Cycling performance of NCM||graphite all-solid-state full cells employing PI–$Li_6PS_5Cl_{0.5}Br_{0.5}$ membranes at 0.1C and 30 °C. Reproduced with permission [151]. Copyright 2020, Elsevier Publications. (g) Schematic illustration of Li plating/stripping processes in NCM||Li batteries based on different electrolyte systems. Reproduced with permission [152]. Copyright 2020, American Chemical Society.

into a PI matrix (Fig. 18g), and the resulting membrane had a thickness of ~ 20 μm and an ionic conductivity of 1.23×10^{-4} S cm^{-1} [152]. The final NCM||Li pouch cells with such an electrolyte exhibited excellent cyclic stability (152.6 mAh g^{-1}, with a capacity retention of 94.9% at 0.1C after 80 cycles) at RT, high functionality, and good safety (withstanding harsh environments such as folding, cutting, and nail penetration).

7. Summary and perspectives

With the ever-increasing growth of the EV market, safety issues and high energy density are now two major concerns. PI-based separators display exceptional thermal stability, excellent mechanical strength, and good chemical stability and thus are promising substitutes for the extensively used PP and PE separators in commercial LIBs. In this review, the recent advances in PI-based separators are summarized, with a special focus on their molecular design and microstructural control. Their physical and electrochemical properties, together with their performance in LIBs, are also discussed. In general, PI-based separators can endure temperatures well above 300 °C. As a result, they can prevent any short circuiting arising from thermal shrinkage of the membrane. Usually, this safety performance originating from the thermal aspect is less relevant to the molecular or micro- structures of PI separators because the maximum operating temperature of liquid electrolytes is usually below the T_g of PIs. However, the molecular design and microstructural control have substantial impacts on other properties of the separators, such as the wettability of the electrolyte, liquid uptake, and ionic conductivity, which eventually determine the performance of the batteries. Therefore, PI separators need to be tailored both on the molecular level and from the microstructural aspect. In terms of molecular design, functional groups should be incorporated to increase the affinity of solvent molecules to PIs for enhancing their wettability by the electrolyte. At the microstructural level, the design of pore structures should complement the mechanical strength, liquid uptake, and dendrite suppression without compromising the ionic conductivity.

Apart from being used in LIBs, PIs have also been extensively studied as separators for novel battery chemistries beyond Li-ion. These advances are reviewed in this paper as well. For LMBs, PIs have been designed as intelligent separators or host materials that can detect or mitigate the growth of dendrites. For LSBs, PIs have been found to strongly adsorb Li polysulfides and therefore are used to mitigate the shuttle effect and reduce self-discharge and capacity decrease. For SSBs, PIs have been either modified at the molecular level or composited with other Li conductors to resolve the conductivity issue. Various design strategies to obtain novel SEs with superior mechanical properties have been discussed.

As mentioned above, after the two decades of effort, PI separator development has witnessed great achievements. Batteries with PI separators now display acceptable performance and are used in some niche applications. Nevertheless, several technological and engineering issues remain unsolved, such as lowering the price and increasing production efficiency. In addition, many questions are yet to be answered to facilitate the design of PI-based separators for LIBs and advanced chemistries beyond Li-ion. These aspects leave wide open some noteworthy opportunities for future development. Some of the most important directions for future research and development in the perspective of the current review are:

1) The interaction between PIs and Li^+ must be investigated at an atomic level. At the moment, some evidence indicates that Li^+ ions might actually be transported in PIs. For example, PIs have been used as both active and coating materials in LIB cathodes. Only when Li^+ diffuses throughout the structure can the corresponding LIB operate. Therefore, it is intriguing to ask how PIs interact with Li^+ at the atomic level and how these interactions influence the properties related to the performance of LIBs, including Li^+ diffusion and electrochemical stability. Answering these questions will not only enable the design of better separators of LIBs but also facilitate the use of PIs in other advanced batteries such as SSBs.
2) The molecular design of PIs should focus on controlling their solubility. Currently, most PIs are almost insoluble in common solvents such as DMAc, EC, and DMC, whereas the precursor PAA is. This would enable PIs to function as separators without dissolving into the electrolyte. However, it also presents difficulties in the fabrication of PI-modified separators because of the relatively poor endurance of the supporting polymers as PAA needs to be thermally activated at temperatures as high as 300 °C to obtain PI.
3) A general framework for designing the microstructures of PI separators needs to be developed. The microstructure of conventional polyolefin-based separators has been designed and iterated based on years of data from both labs and the industry. Research on the influence of the microstructure on the performance of PI-based separators is still scarce. In fact, the ideal pore structure that enables PI separators with high mechanical strength, high liquid uptake, and ease of fabrication is still unknown.
4) Methods must be developed to lower the cost of PI-based separators and to speed up large-scale production. Many PI-based separators fabricated in labs already meet the industrial requirements of LIBs. However, the fabrication is still too expensive for large-scale use compared with their polyolefin-based counterparts. The overly high price has two origins. First, the precursor for PI is more expensive than that for polyolefins. Second, and more importantly, fabrication methods, such as electrospinning and phase inversion, are either too slow or too difficult to control. Therefore, these methods are more suitable for lab-scale research than industrial-scale production. It is therefore important to seek methods that will enable the fabrication of PI-based separators at a low cost to make them competitive from a commercial standpoint.
5) High-value-added products are welcome in the area of PI-based separators. As PI-based products might inevitably be associated with high production costs before any technological or engineering breakthrough, a reasonable strategy is to find applications for them in fields with a high profit margin. In this regard, intelligent fire-extinguishing separators for safe batteries, dendrite-suppressing separators for LMBs, polysulfide-absorbing separators for LSBs, and SEs for SSBs are promising directions for future research.

Declaration of Competing Interest

The authors declare that they have no known competing financial interests or personal relationships that could have appeared to influence the work reported in this paper.

Acknowledgments

This work was supported by the Basic Research Program of Shenzhen (No. JCYJ20190812161409163), the Basic and Applied Basic Research Program of Guangdong Province (No. 2019A1515110531), and the SIAT Innovation Program for Excellent Young Researchers.

References

[1] M. Armand, J.-M. Tarascon, Nature 451 (2008) 652–657.
[2] M. Winter, B. Barnett, K. Xu, Chem. Rev. 118 (2018) 11433–11456.
[3] K. Xu, Chem. Rev. 104 (2004) 4303–4418.
[4] K. Xu, Chem. Rev. 114 (2014) 11503–11618.
[5] J. Lee, Y. Lee, J. Lee, S.-M. Lee, J.-H. Choi, H. Kim, M.-S. Kwon, K. Kang, K.T. Lee, N.-S. Choi, A.C.S. Appl, Mater. Interfaces 9 (2017) 3723–3732.
[6] C. Yi, W. Li, S. Shi, K. He, P. Ma, M. Chen, C. Yang, Solar Energy 195 (2020) 340–354.
[7] P. Ma, C. Dai, H. Wang, Z. Li, H. Liu, W. Li, C. Yang, Compos. Commun. 16 (2019) 84–93.
[8] Y. Ding, H. Hou, Y. Zhao, Z. Zhu, H. Fong, Prog. Polym. Sci. 61 (2016) 67–103.
[9] S.H. Yoo, J.H. Kim, J.Y. Jho, J. Won, Y.S. Kang, J. Membrane Sci. 236 (2004) 203–207.
[10] W. Kim, M.-K. Lee, Mater. Lett. 63 (2009) 933–936.
[11] Z. Ahmad, J. Mark, Chem. Mater. 13 (2001) 3320–3330.
[12] P. Arora, Z. Zhang, Chem. Rev. 104 (2004) 4419–4462.
[13] V. Deimede, C. Elmasides, Energy Technol. 3 (2015) 453–468.
[14] M. Li, C. Wang, Z. Chen, K. Xu, J. Lu, Chem. Rev. 120 (2020) 6783–6819.
[15] Y. Yamada, J. Wang, S. Ko, E. Watanabe, A. Yamada, Nat. Energy 4 (2019) 269–280.
[16] C.F. Francis, I.L. Kyratzis, A.S. Best, Adv. Mater. 32 (2020) 1904205.
[17] I. Osada, H. de Vries, B. Scrosati, S. Passerini, Angew. Chem. Int. Ed. 55 (2016) 500–513.
[18] K. Abraham, Electrochim. Acta 38 (1993) 1233–1248.
[19] H. Lee, M. Yanilmaz, O. Toprakci, K. Fu, X. Zhang, Energy Environ. Sci. 7 (2014) 3857–3886.
[20] M.F. Lagadec, R. Zahn, V. Wood, Nat. Energy 4 (2019) 16–25.
[21] M. Yang, J. Hou, Membranes 2 (2012) 367–383.
[22] G. Sun, B. Liu, H. Niu, F. Hao, N. Chen, M. Zhang, G. Tian, S. Qi, D. Wu, J. Membrane Sci. 595 (2020) 117509.
[23] L. Kong, B. Liu, J. Ding, X. Yan, G. Tian, S. Qi, D. Wu, J. Membrane Sci. 549 (2018) 244–250.
[24] X. Zhou, L. Yue, J. Zhang, Q. Kong, Z. Liu, J. Yao, G. Cui, J. Electrochem. Soc. 160 (2013) A1341–A1347.
[25] C.J. Orendorff, T.N. Lambert, C.A. Chavez, M. Bencomo, K.R. Fenton, Adv. Energy Mater. 3 (2013) 314–320.
[26] J. Hao, G. Lei, Z. Li, L. Wu, Q. Xiao, L. Wang, J. Membrane Sci. 428 (2013) 11–16.
[27] W. Qi, C. Lu, P. Chen, L. Han, Q. Yu, R. Xu, Mater. Lett. 66 (2012) 239–241.
[28] Q. Xu, Q. Kong, Z. Liu, X. Wang, R. Liu, J. Zhang, L. Yue, Y. Duan, G. Cui, A.C.S. Sustain, Chem. Eng. 2 (2014) 194–199.
[29] T.-H. Cho, M. Tanaka, H. Ohnishi, Y. Kondo, M. Yoshikazu, T. Nakamura, T. Sakai, J. Power Sources 195 (2010) 4272–4277.
[30] P. Carol, P. Ramakrishnan, B. John, G. Cheruvally, J. Power Sources 196 (2011) 10156–10162.
[31] G. Maier, Prog. Polym. Sci. 26 (2001) 3–65.
[32] W.-W. Cui, D.-Y. Tang, Y.-S. Lu, N. Zhang, L.-Z. Liu, J.-L. Mu, Iranian Polymer Journal 26 (2017) 179–191.
[33] J. Lee, J. Kim, Polymers 12 (2020) 721.
[34] D.J. Liaw, K.L. Wang, Y.C. Huang, K.R. Lee, J.Y. Lai, C.S. Ha, Prog. Polym. Sci. 37 (2012) 907–974.
[35] P.K. Tapaswi, C.-S. Ha, Macromol. Chem. Phys. 220 (2019) 1800313.
[36] M. Hasegawa, Polymers 9 (2017) 520.
[37] M. Fryd, in: Polyimides, Springer US, Boston, MA, 1984, pp. 377–383, https://doi.org/10.1007/978-1-4615-7637-2_25.
[38] D. Ayala, A.E. Lozano, J. De Abajo, J.G. De La Campa, J. Polym. Sci. Polym. Chem. 37 (1999) 805–814.
[39] D.J. Liaw, P.N. Hsu, W.H. Chen, B.Y. Liaw, Macromol. Chem. Phys. 202 (2001) 1483–1487.
[40] K. Kudo, T. Imai, T. Hamada, S. Sakamoto, High Perform. Polym. 18 (2006) 749–759.
[41] S. Sasaki, S. Nishi, Synthesis of flurinated polyimides, in: M.K. Ghosh, K.L. Mittal (Eds.), Polyimides: fundamentals and applications, Marcel Dekker, New York, 1996, p. 71.
[42] J.-H. Kim, J.-H. Kim, K.-H. Choi, H.K. Yu, J.H. Kim, J.S. Lee, S.-Y. Lee, Nano Lett. 14 (2014) 4438–4448.
[43] Y. Maeyoshi, D. Ding, M. Kubota, H. Ueda, K. Abe, K. Kanamura, H. Abe, A.C.S. Appl, Mater. Interfaces 11 (2019) 25833–25843.
[44] Y. Maeyoshi, S. Miyamoto, H. Munakata, K. Kanamura, J. Power Sources 350 (2017) 103–108.
[45] Y. Shimizu, K. Kanamura, J. Electrochem. Soc. 166 (2019) A754–A761.
[46] D. Lin, D. Zhuo, Y. Liu, Y. Cui, J. Am. Chem. Soc. 138 (2016) 11044–11050.
[47] H. Zhang, C.-E. Lin, M.-Y. Zhou, A.E. John, B.-K. Zhu, Electrochim. Acta 187 (2016) 125–133.
[48] M. Li, Z. Zhang, Y. Yin, W. Guo, Y. Bai, F. Zhang, B. Zhao, F. Shen, X. Han, A.C.S. Appl, Mater. Interfaces 12 (2020) 3610–3616.
[49] G.R. Guillen, Y. Pan, M. Li, E.M. Hoek, Ind. Eng. Chem. Res. 50 (2011) 3798–3817.
[50] H. Wang, T. Wang, S. Yang, L. Fan, Polymer 54 (2013) 6339–6348.
[51] C.-E. Lin, H. Zhang, Y.-Z. Song, Y. Zhang, J.-J. Yuan, B.-K. Zhu, J. Mater. Chem. A 6 (2018) 991–998.
[52] J. Wan, J. Xie, X. Kong, Z. Liu, K. Liu, F. Shi, A. Pei, H. Chen, W. Chen, J. Chen, X. Zhang, L. Zong, J. Wang, L.-Q. Chen, J. Qin, Y. Cui, Nat. Nanotechnol. 14 (2019) 705–711.
[53] B. Zhang, F. Kang, J.-M. Tarascon, J.-K. Kim, Prog. Mater. Sci. 76 (2016) 319–380.
[54] D. Li, Y. Xia, Adv. Mater. 16 (2004) 1151–1170.
[55] Z.-M. Huang, Y.-Z. Zhang, M. Kotaki, S. Ramakrishna, Compos. Sci. Technol. 63 (2003) 2223–2253.
[56] D.H. Reneker, I. Chun, Nanotechnology 7 (1996) 216.
[57] Y.-E. Miao, G.-N. Zhu, H. Hou, Y.-Y. Xia, T. Liu, J. Power Sources 226 (2013) 82–86.
[58] W. Jiang, Z. Liu, Q. Kong, J. Yao, C. Zhang, P. Han, G. Cui, Solid State Ion. 232 (2013) 44–48.
[59] J. Hou, W. Jang, S. Kim, J.-H. Kim, H. Byun, RSC Adv. 8 (2018) 14958–14966.
[60] L. Kong, L. Yuan, B. Liu, G. Tian, S. Qi, D. Wu, J. Electrochem. Soc. 164 (2017) A1328–A1332.
[61] S. Byun, S.H. Lee, D. Song, M.-H. Ryou, Y.M. Lee, W.H. Park, J. Ind. Eng. Chem. 72 (2019) 390–399.
[62] L. Kong, Y. Yan, Z. Qiu, Z. Zhou, J. Hu, J. Membrane Sci. 549 (2018) 321–331.
[63] D. Wang, J. Yu, G. Duan, K. Liu, H. Hou, J. Mater. Sc. 55 (2020) 5667–5679.
[64] S. Chen, P. Hu, A. Greiner, C. Cheng, H. Cheng, F. Chen, H. Hou, Nanotechnology 19 (2007) 015604.
[65] J. Li, K. Luo, J. Yu, Y. Wang, J. Zhu, Z. Hu, Ind. Eng. Chem. Res. 57 (2018) 12296–12305.
[66] Y. Li, Q. Li, Z. Tan, J. Power Sources 443 (2019) 227262.
[67] J.-W. Jung, C.-L. Lee, S. Yu, I.-D. Kim, J. Mater. Chem. A 4 (2016) 703–750.
[68] J. Song, M.-H. Ryou, B. Son, J.-N. Lee, D.J. Lee, Y.M. Lee, J.W. Choi, J.-K. Park, Electrochim. Acta 85 (2012) 524–530.
[69] G. Kim, J. Kim, J. Jeong, D. Lee, M. Kim, S. Lee, S. Kim, H. Lee, H. Han, Int. J. Electrochem. Sci. 14 (2019) 7133–7148.
[70] Y. Lee, H. Lee, T. Lee, M.-H. Ryou, Y.M. Lee, J. Power Sources 294 (2015) 537–544.
[71] J. Ding, Y. Kong, P. Li, J. Yang, J. Electrochem. Soc. 159 (2012) A1474–A1480.
[72] B. Zhang, Q. Wang, J. Zhang, G. Ding, G. Xu, Z. Liu, G. Cui, Nano Energy 10 (2014) 277–287.
[73] W.U. Arifeen, M. Kim, D. Ting, R. Kurniawan, J. Choi, K. Yoo, T.J. Ko, Mater. Chem. Phys. 245 (2020) 122780.
[74] G. Dong, G. Sun, G. Tian, S. Qi, D. Wu, Energy Technol. 7 (2019) 1801072.
[75] X. Liang, Y. Yang, X. Jin, J. Cheng, J. Mater. Sci. Technol. 32 (2016) 200–206.
[76] C.-T. Hsieh, S.-C. Lin, C.-H. Lee, C.-F. Liu, C.-C. Hu, J. Electrochem. Soc. 166 (2019) A3132–A3138.
[77] G. Sun, L. Kong, B. Liu, H. Niu, M. Zhang, G. Tian, S. Qi, D. Wu, J. Membrane Sci. 582 (2019) 132–139.
[78] M. Cai, J.W. Zhu, C.C. Yang, R.Y. Gao, C. Shi, J.B. Zhao, Polymers 11 (2019) 185.
[79] S. Park, C.W. Son, S. Lee, D.Y. Kim, C. Park, K.S. Eom, T.F. Fuller, H.I. Joh, S.M. Jo, Sci. Rep. 6 (2016) 36977.
[80] W. Chen, Y. Liu, Y. Ma, W. Yang, J. Power Sources 273 (2015) 1127–1135.
[81] W. Chen, Y. Liu, Y. Ma, J. Liu, X. Liu, Mater. Lett. 133 (2014) 67–70.
[82] Z. Liu, W. Jiang, Q. Kong, C. Zhang, P. Han, X. Wang, J. Yao, G. Cui, Macromol. Mater. Eng. 298 (2013) 806–813.
[83] C. Shi, P. Zhang, S. Huang, X. He, P. Yang, D. Wu, D. Sun, J. Zhao, J. Power Sources 298 (2015) 158–165.
[84] D. Wu, C. Shi, S. Huang, X. Qiu, H. Wang, Z. Zhan, P. Zhang, J. Zhao, D. Sun, L. Lin, Electrochim. Acta 176 (2015) 727–734.
[85] C. Shi, P. Zhang, L. Chen, P. Yang, J. Zhao, J. Power Sources 270 (2014) 547–553.
[86] X. Liang, Y. Yang, X. Jin, Z. Huang, F. Kang, J. Membrane Sci. 493 (2015) 1–7.
[87] G. Dong, B. Liu, L. Kong, Y. Wang, G. Tian, S. Qi, D. Wu, A.C.S. Sustain, Chem. Eng. 7 (2019) 17643–17652.
[88] G. Zhong, Y. Wang, C. Wang, Z. Wang, S. Guo, L. Wang, X. Liang, H. Xiang, Ionics 25 (2019) 2677–2684.
[89] G. Sun, G. Dong, L. Kong, X. Yan, G. Tian, S. Qi, D. Wu, Nanoscale 10 (2018) 22439–22447.
[90] L. Wang, F. Liu, W. Shao, S. Cui, Y. Zhao, Y. Zhou, J. He, Compos. Commun. 16 (2019) 150–157.
[91] S. Cheng, D. Shen, X. Zhu, X. Tian, D. Zhou, L.-J. Fan, Eur. Polym. J. 45 (2009) 2767–2778.
[92] Y. Wang, S. Wang, J. Fang, L.-X. Ding, H. Wang, J. Membrane Sci. 537 (2017) 248–254.
[93] K. Song, Y. Huang, X. Liu, Y. Jiang, P. Zhang, Y. Ding, J. Sol-Gel Sci. Technol. (2019) 1–9.
[94] J. Lee, C.-L. Lee, K. Park, I.-D. Kim, J. Power Sources 248 (2014) 1211–1217.
[95] G. Dong, B. Liu, G. Sun, G. Tian, S. Qi, D. Wu, J. Membrane Sci. 577 (2019) 249–257.
[96] G. Dong, N. Dong, B. Liu, G. Tian, S. Qi, D. Wu, J. Membrane Sci. 601 (2020) 117884.
[97] J. Liu, Y.B. Liu, W.X. Yang, Q. Ren, F.Y. Li, Z. Huang, J. Power Sources 396 (2018) 265–275.
[98] J. Liu, Z. Bao, Y. Cui, E.J. Dufek, J.B. Goodenough, P. Khalifah, Q. Li, B.Y. Liaw, P. Liu, A. Manthiram, Nat. Energy 4 (2019) 180–186.
[99] G.A. Umeda, E. Menke, M. Richard, K.L. Stamm, F. Wudl, B. Dunn, J. Mater. Chem. 21 (2011) 1593–1599.
[100] Y.M. Lee, J.E. Seo, Y.G. Lee, S.H. Lee, K.Y. Cho, J.K. Park, Electrochem. Solid-State Lett. 10 (2007) 216–219.
[101] S.S. Zhang, J. Power Sources 162 (2006) 1379–1394.
[102] L. Gireaud, S. Grugeon, S. Laruelle, B. Yrieix, J.M. Tarascon, Electrochem. Commun. 8 (2006) 1639–1649.
[103] M.Z. Mayers, J.W. Kaminski, T.F. Miller, J. Phys. Chem. C 116 (2012) 26214–26221.

[104] K.P. Doyle, C.M. Lang, K. Kim, P.A. Kohl, J. Electrochem. Soc. 153 (2006) A1353–A1357.
[105] Z. Shi, M. Liu, D. Naik, J.L. Gole, J. Power Sources 92 (2001) 70–80.
[106] C. Monroe, J. Newman, J. Electrochem. Soc. 150 (2003) A1377–A1384.
[107] C. Monroe, J. Newman, J. Electrochem. Soc. 151 (2004) A880–A886.
[108] C. Monroe, J. Newman, J. Electrochem. Soc. 152 (2005) A396–A404.
[109] H. Munakata, D. Yamamoto, K. Kanamura, J. Power Sources 178 (2008) 596–602.
[110] M. Nagasaki, K. Kanamura, A.C.S. Appl, Energy Mater. 2 (2019) 3896–3903.
[111] K. Kanamura, H. Munakata, S. Ochiai, ECS Trans. 1 (2006) 161.
[112] D. Kim, H. Munakata, J. Park, Y. Roh, D. Jin, M.-H. Ryou, K. Kanamura, Y.M. Lee, A.C.S. Appl, Energy Mater. 3 (2020) 3721–3727.
[113] W. Liu, D. Lin, A. Pei, Y. Cui, J. Am. Chem. Soc. 138 (2016) 15443–15450.
[114] Y. Liu, D. Lin, Z. Liang, J. Zhao, K. Yan, Y. Cui, Nat. Commun. 7 (2016) 10992.
[115] P. Zou, Y. Wang, S.-W. Chiang, X. Wang, F. Kang, C. Yang, Nat. Commun. 9 (2018) 464.
[116] J. Yi, J. Chen, Z. Yang, Y. Dai, W. Li, J. Cui, F. Ciucci, Z. Lu, C. Yang, Adv. Energy Mater. 9 (2019) 1901796.
[117] R. Fang, S. Zhao, Z. Sun, D.W. Wang, H.M. Cheng, F. Li, Adv. Mater. 29 (2017) 1606823.
[118] H.J. Peng, J.Q. Huang, X.B. Cheng, Q. Zhang, Adv. Energy Mater. 7 (2017) 1700260.
[119] Q. Pang, X. Liang, C.Y. Kwok, L.F. Nazar, Nat. Energy 1 (2016) 16132.
[120] W. Kang, N. Deng, J. Ju, Q. Li, D. Wu, X. Ma, L. Li, M. Naebe, B. Cheng, Nanoscale 8 (2016) 16541–16588.
[121] Y. Jiang, F. Chen, Y. Gao, Y. Wang, S. Wang, Q. Gao, Z. Jiao, B. Zhao, Z. Chen, J. Power Sources 342 (2017) 929–938.
[122] Y. Wang, Z. Zhang, M. Haibara, D. Sun, X. Ma, Y. Jin, H. Munakata, K. Kanamura, Electrochim. Acta 255 (2017) 109–117.
[123] X. Luo, X. Lu, G. Zhou, X. Zhao, Y. Ouyang, X. Zhu, Y.-E. Miao, T. Liu, A.C.S. Appl, Mater. Interfaces 10 (2018) 42198–42206.
[124] L. Wang, N. Deng, L. Fan, L. Wang, G. Wang, W. Kang, B. Cheng, Mater. Lett. 233 (2018) 224–227.
[125] M. Rao, X. Li, Y. Liao, X. Li, W. Li, Ionics 21 (2015) 1937–1943.
[126] Z. Zhou, Y. Li, T. Fang, Y. Zhao, Q. Wang, J. Zhang, Z. Zhou, Nanomaterials 9 (2019) 1574.
[127] M.-J. Kim, K. Yang, H.-J. Kang, H.J. Hwang, J.C. Won, Y.H. Kim, Y.-S. Jun, Nanomaterials 9 (2019) 1612.
[128] Y. Li, J. Zhang, C. Zhou, M. Ling, J. Lu, Y. Hou, Q. Zhang, Q. He, X. Zhan, F. Chen, J. Alloys Compd. 826 (2020) 154197.
[129] L. Kong, X. Fu, X. Fan, Y. Wang, S. Qi, D. Wu, G. Tian, W.-H. Zhong, Nanoscale 11 (2019) 18090–18098.
[130] Y. Wang, J. He, Z. Zhang, Z. Liu, C. Huang, Y. Jin, A.C.S. Appl, Mater. Interfaces 11 (2019) 35738–35745.
[131] Z. Zhou, T. Zhao, X. Lu, H. Cao, X. Zha, Z. Zhou, J. Power Sources 396 (2018) 542–550.
[132] Z. Song, H. Zhan, Y. Zhou, Angew. Chem. Int. Ed. 49 (2010) 8444–8448.
[133] Y. Liang, Z. Tao, J. Chen, Adv. Energy Mater. 2 (2012) 742–769.
[134] B. Haeupler, A. Wild, U.S. Schubert, Adv. Energy Mater. 5 (2015) 1402034.
[135] S. Muench, A. Wild, C. Friebe, B. Häupler, T. Janoschka, U.S. Schubert, Chem. Rev. 116 (2016) 9438–9484.
[136] P.-Y. Gu, Y. Zhao, J. Xie, N. Binte Ali, L. Nie, Z.J. Xu, Q. Zhang, A.C.S. Appl, Mater. Interfaces 8 (2016) 7464–7470.
[137] G. Hernández, N. Lago, D. Shanmukaraj, M. Armand, D. Mecerreyes, Mater. Today, Energy 6 (2017) 264–270.
[138] J. Wang, Y. Yang, F. Kang, Electrochim. Acta 168 (2015) 271–276.
[139] T. Pakki, E.H. Mohan, N.Y. Hebalkar, J. Adduru, S.V. Bulusu, A. Srinivasan, K.M. Mantravadi, N.R. Tata, J. Mater. Sc. 54 (2019) 9075–9087.
[140] Q. Zhao, S. Stalin, C.-Z. Zhao, L.A. Archer, Nat. Rev. Mater. 5 (2020) 229–252.
[141] A. Manthiram, X. Yu, S. Wang, Nat. Rev. Mater. 2 (2017) 16103.
[142] Z. Xue, D. He, X. Xie, J. Mater. Chem. A 3 (2015) 19218–19253.
[143] M.A.B. Meador, V.A. Cubon, D.A. Scheiman, W.R. Bennett, Chem. Mater. 15 (2003) 3018–3025.
[144] C. Xue, M.A.B. Meador, L. Zhu, J.G. Jason, S.Z. Cheng, S. Putthanarat, R. Eby, A. Khalfan, G.D. Bennett, S.G. Greenbaum, Polymer 47 (2006) 6149–6155.
[145] M. Higa, K. Yaguchi, R. Kitani, Electrochim. Acta 55 (2010) 1380–1384.
[146] R.D. Toker Öztürk, M.H. Uğur, A. Gungor, N. Kayaman-Apohan, Adv. Polym. Tech. 37 (2018) 1356–1365.
[147] Z. Zou, Y. Li, Z. Lu, D. Wang, Y. Cui, B. Guo, Y. Li, X. Liang, J. Feng, H. Li, Chem. Rev. 120 (2020) 4169–4221.
[148] S. Shi, J. Gao, Y. Liu, Y. Zhao, Q. Wu, W. Ju, C. Ouyang, R. Xiao, Chin. Phys. B 25 (2015) 018212.
[149] Y. Cui, J. Wan, Y. Ye, K. Liu, L.-Y. Chou, Y. Cui, Nano Lett. 20 (2020) 1686–1692.
[150] K. Liu, Q. Zhang, B.P. Thapaliya, X.-G. Sun, F. Ding, X. Liu, J. Zhang, S. Dai, Solid State Ion. 345 (2020) 115159.
[151] J. Hu, P. He, B. Zhang, B. Wang, L.Z. Fan, Energy Storage Mater. 26 (2020) 283–289.
[152] D.H. Kim, Y.-H. Lee, Y.B. Song, H. Kwak, S.-Y. Lee, Y.S. Jung, ACS Energy Lett. 5 (2020) 718–727.

Ziheng Lu received his B.S. from the Nanjing University of Science and Technology, China in 2014 and earned his Ph.D. from the Hong Kong University of Science and Technology in 2018. He joined the Shenzhen Institutes of Advanced Technology, Chinese Academy of Sciences as an assistant professor afterwards. His current research focuses on computational-aided design of materials and interfaces for solid-state batteries as well as laser-assisted synthesis of novel compounds for energy storage and conversion.

Fan Sui received her B.S. degree from Hunan University in 2010 and Ph.D. degree from University of California, Davis in 2016. She joined Shenzhen Institutes of Advanced Technology, Chinese Academy of Sciences as assistant professor since 2016. Her main research interests include crystallography and chemistry of inorganic materials, new fluorescent nanocrystals and optoelectronic devices.

Yue-E Miao received her B.S. degree from Southeast University in 2010 and Ph.D. degree from Fudan University in 2015. She is now an associate professor of School of Materials Science and Engineering at Donghua University. Her research interests mainly focus on high-performance organic fiber electrodes/separators, carbon nanofiber composites, as well as their applications in electrochemical energy storage devices (such as Li/Na-ion batteries, and Li–S batteries)

Guohua Liu is currently studying as master student in University of Science and Technology of China (USTC). She works on electrochemical energy storage at the Shenzhen Institute of Advanced Technology, Chinese Academy of Sciences.

Cheng Li is pursuing his master degree in University of Science and Technology of China (USTC) and is doing his research in Shenzhen Institutes of Advanced Technology, Chinese Academy of Sciences. His research interests focus on all solid-state lithium-ion batteries and the interfaces.

Wei Dong is studying for a master's degree at the University of Science and Technology of China, and since July 2020 he joined the Shenzhen Institute of Advanced Technology, Chinese Academy of Sciences. His research focuses on anode-free solid-state lithium batteries.

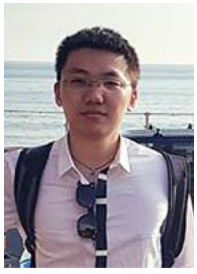

Jiang Cui received his B.E. from Xi'an Jiaotong University, China in 2014. He earned his Ph.D. in 2018 from the Hong Kong University of Science and Technology. He is currently working as a Postdoctoral Fellow at the Clemson University, USA. His research interests lie primarily in studying the fundamental mechanisms of energy materials by electrochemistry, *in-situ* TEM, and first-principles calculations.

Tianxi Liu obtained his BS degree from Henan University (1992) and Ph.D. degree from Changchun Institute of Applied Chemistry, Chinese Academy of Sciences (1998). He is currently a full professor in Donghua University. His main research interests include polymer nanocomposites, organic/ inorganic hybrid materials, nanofibers and their composites, advanced energy materials for energy conversion and storage.

Junxiong Wu received his B. S. from Fuzhou University and M.E. from Tsinghua University in 2013 and 2016, respectively, and completed his Ph.D. at the Hong Kong University of Science and Technology in 2020. He is currently a postdoctoral researcher at the Hong Kong Polytechnic University. His research focuses on new materials for Li/Na-ion batteries and alkali metal anodes.

Chunlei Yang received his Ph.D. degree in physics from the Hong Kong University of Science and Technology in 2005. He joined Shenzhen Institutes of Advanced Technology, Chinese Academy of Sciences in 2010 as a full professor. He is the director of the Center for Photonics Information and Energy Materials. His research focuses on the fabrication and characterization of semiconductors and relevant devices.